RESEARCH ARTICLE

MULTIPLE SCLEROSIS

A noninflammatory mRNA vaccine for treatment of experimental autoimmune encephalomyelitis

Christina Krienke[1,2], Laura Kolb[1]*, Elif Diken[1]*, Michael Streuber[1], Sarah Kirchhoff[1], Thomas Bukur[1], Özlem Akilli-Öztürk[1], Lena M. Kranz[3], Hendrik Berger[3], Jutta Petschenka[1,4], Mustafa Diken[1,3], Sebastian Kreiter[1,3], Nir Yogev[5,6], Ari Waisman[2,5], Katalin Karikó[3], Özlem Türeci[3,7], Ugur Sahin[1,2,3]†

The ability to control autoreactive T cells without inducing systemic immune suppression is the major goal for treatment of autoimmune diseases. The key challenge is the safe and efficient delivery of pharmaceutically well-defined antigens in a noninflammatory context. Here, we show that systemic delivery of nanoparticle-formulated 1 methylpseudouridine-modified messenger RNA (m1Ψ mRNA) coding for disease-related autoantigens results in antigen presentation on splenic CD11c$^+$ antigen-presenting cells in the absence of costimulatory signals. In several mouse models of multiple sclerosis, the disease is suppressed by treatment with such m1Ψ mRNA. The treatment effect is associated with a reduction of effector T cells and the development of regulatory T cell (T_{reg} cell) populations. Notably, these T_{reg} cells execute strong bystander immunosuppression and thus improve disease induced by cognate and noncognate autoantigens.

Antigen-specific tolerization for the treatment of autoimmune diseases may selectively blunt autoimmunity without compromising normal immune function. In the past decades, various approaches have been studied, including delivery of autoimmune antigens using DNA, synthetic peptides, recombinant proteins, coated nanoparticles, or immunomodulatory cellular therapies [reviewed in (*1*)]. However, clinical translation remained elusive, with largely negative or inconclusive outcomes in human studies, and only a few approaches are in early clinical testing. One impediment is the polyclonal complexity of autoimmune diseases driven by distinctive, diverse autoreactive immune cell repertoires of patients. The interindividual variability requires either personalized treatment tailored for the autoantigenic immune profiles of the patients or therapies that mediate bystander tolerance to suppress both cognate and noncognate autoimmune lymphocytes without broad immune suppression (*2*).

[1]TRON – Translational Oncology at the University Medical Center of the Johannes Gutenberg University gGmbH, Freiligrathstr. 12, Mainz 55131, Germany. [2]Research Center for Immunotherapy (FZI), University Medical Center at the Johannes Gutenberg University, Langenbeckstr. 1, Mainz 55131, Germany. [3]Biopharmaceutical New Technologies (BioNTech) Corporation, An der Goldgrube 12, Mainz 55131, Germany. [4]Cancer Immunology and Immune Modulation, Boehringer Ingelheim Pharma GmbH & Co. KG, Birkendorfer Str. 65, 88397 Biberach an der Riss, Germany. [5]Institute for Molecular Medicine, University Medical Center of the Johannes Gutenberg University, Mainz 55131, Germany. [6]Clinic and Polyclinic for Dermatology and Venereology, University Hospital Cologne, Kerpenerstr. 62, Cologne 50937, Germany. [7]CI3 – Cluster for Individualized Immunointervention e.V., Hölderlinstraße 8, 55131 Mainz, Germany.
*These authors contributed equally to this work.
†Corresponding author. Email: sahin@uni-mainz.de

The physiological induction and maintenance of peripheral tolerance is based on the presentation of self-antigens by lymphoid antigen-presenting cells (APCs) with low-level surface expression of costimulatory molecules, such as CD86. We sought to develop a therapeutic approach that would emulate natural mechanisms of immune tolerance. We recently introduced a liposomal formulation for systemic delivery of mRNA-encoded vaccine antigens (mRNA-LPX) into lymphoid tissue-resident CD11c$^+$ APCs (*3*). mRNA vaccination induces strong type 1 T helper (T_H1) cell responses driven by high levels of interferon-α (IFN-α), released from APCs upon Toll-like receptor (TLR) signaling (*3*). Replacement of uridine (U) by incorporation of 1-methylpseudouridine (m1Ψ) during in vitro transcription and subsequent removal of double-stranded mRNA contaminants is known to abrogate TLR7-triggering activity and to reduce inflammatory properties of single-stranded mRNA (*4*–*6*). We hypothesized that the use of such nucleoside-modified, purified mRNA (m1Ψ mRNA) for in vivo delivery of autoimmune disease target antigens into CD11c$^+$ APCs in a noninflammatory context would enable systemic tolerogenic antigen presentation in lymphoid tissues.

Noninflammatory delivery of antigen-encoding m1Ψ mRNA into the spleen expands antigen-specific CD4$^+$ regulatory T cells

To test this hypothesis, we engineered nanoparticle-formulated mRNA-LPX (herein referred to as mRNA) consisting of nonimmunogenic (m1Ψ) or immunogenic (U) mRNA complexed with liposomes that lack inherent adjuvant activity. In a first experiment, mRNA coding for the reporter gene firefly luciferase (LUC) or saline as control was administered intravenously into albino C57BL/6 mice, and the translation and expression of the LUC protein was assessed.

In line with previous reports, administration of U mRNA led to strong activation of CD11c$^+$ APCs and lymphocytes, and secretion of high levels of IFN-α (Fig. 1, A to C, and fig. S1, A and B). By contrast, we did not observe secretion of IFN-α or other inflammatory cytokines or significant activation of CD11c$^+$ APCs, CD8$^+$ and CD4$^+$ T cells, or natural killer (NK) and B cells in m1Ψ mRNA–treated mice (Fig. 1, A to C, and fig. S1, A and B). Notably, translation of LUC was profoundly higher and prolonged in m1Ψ mRNA–treated animals (Fig. 1, D and E). These findings suggest that m1Ψ mRNA is suitable for noninflammatory delivery of proteins into splenic CD11c$^+$ APCs.

To study the effects of m1Ψ mRNA in an autoimmune disease, we chose experimental autoimmune encephalomyelitis (EAE), a clinically relevant mouse model of multiple sclerosis (MS), in which we previously demonstrated tolerance induction by selectively expressing MOG_{35-55}, the epitope of myelin oligodendrocyte glycoprotein, in dendritic cells (DCs) (*7*). We assessed the effect of antigen-encoding m1Ψ mRNA treatment on T cell expansion. Naïve Thy1.2$^+$ C57BL/6 mice were immunized with MOG_{35-55} m1Ψ or U mRNA, and the expansion of both endogenous T cells and adoptively transferred MOG_{35-55}–T cell receptor transgenic Thy1.1$^+$ CD4$^+$ T cells from 2D2 mice (*8*) was assessed. Both MOG_{35-55}–encoding mRNAs induced proliferation of adoptively transferred CD4$^+$ 2D2 T cell, with MOG_{35-55} m1Ψ mRNA being superior (Fig. 1F). Similarly, endogenous MOG_{35-55}–specific CD4$^+$ T cells in naïve mice were expanded by both MOG_{35-55}–encoding mRNAs (Fig. 1G). However, the functional properties of the T cells induced with either of these mRNAs differed profoundly. MOG_{35-55} m1Ψ mRNA treatment was capable of expanding or inducing de novo Foxp3$^+$ regulatory T cells (T_{reg} cells) in both wild-type C57BL/6 and 2D2-Foxp3-eGFP transgenic mice (Fig. 1H and fig. S2A), whereas overall frequencies of CD4$^+$ Foxp3$^+$ T cells did not change (Fig. 1H). CD4$^+$ T cells from vaccinated 2D2 animals inhibited the in vitro proliferation of antigen-specific naïve CD4 T cells in a dose-dependent manner. By contrast, CD4$^+$ T cells of MOG_{35-55} U mRNA or control-treated mice showed little to no suppressive activity (fig. S2B).

We studied the cytokine response profiles upon in vitro antigen restimulation and the phenotypes of expanded T cells in repetitively vaccinated C57BL/6 mice in more detail. Whereas MOG_{35-55} U mRNA–expanded T cells exhibited a functional T_H1 effector profile with secretion of IFN-γ, tumor necrosis factor–α (TNFα), interleukin-6 (IL-6), granulocyte-macrophage colony-stimulating factor, and

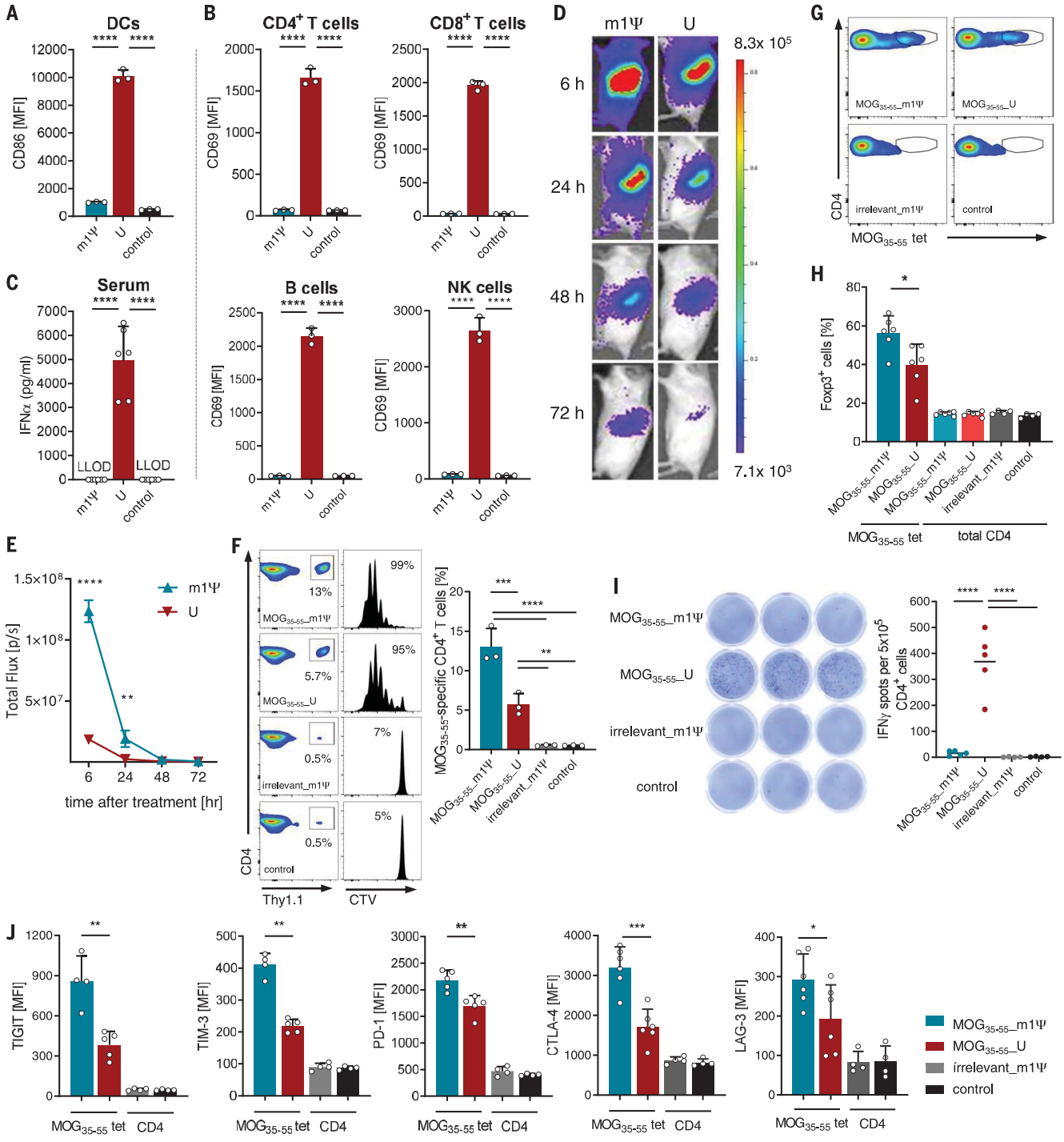

Fig. 1. Antigen-encoding m1Ψ mRNA potently expands antigen-specific CD4$^+$ T_{reg} cells by noninflammatory delivery into the spleen. (**A** and **B**) Activation of splenic immune cells 24 hours after (n = 3) and (**C**) IFN-α serum levels 6 hours after intravenous injection of LPX-formulated mRNAs and saline (control) in C57BL/6 mice (n = 6). (**D** and **E**) Bioluminescence imaging of albino C57BL/6 mice (n = 5) after intravenous injection of m1Ψ or U LUC mRNA. Representative mice are shown. (**F**) Frequency and proliferation profiles of MOG_{35-55}–specific CD4$^+$ T cells isolated from Thy1.1$^+$ 2D2 mice, cell trace violet (CTV)–labeled, and transferred into naïve Thy1.2$^+$ C57BL/6 recipient mice. Twenty-four hours after adoptive cell transfer, C57BL/6 mice were treated with mRNAs or saline (control). Mice were sacrificed on day 4, and spleens were analyzed for proliferating CD4$^+$ Thy1.1$^+$ cells (n = 3). (**G**) Expansion of endogenous MOG_{35-55}–specific CD4$^+$ T cells and (**H**) frequency of splenic Foxp3$^+$ T_{reg} cells (n = 6) in C57BL/6 mice after treatment (days 0, 3, 7, and 10) with mRNA or saline (control) analyzed by MOG_{35-55}–tetramer (tet) staining 3 days after last dosing (n = 4 to 6). (**I**) CD4$^+$ T cells of mice from (G) tested for IFN-γ secretion by enzyme-linked immune absorbent spot (ELISpot) upon restimulation with MOG_{35-55} peptide (n = 4 to 5). (**J**) Phenotype of tet$^+$ CD4$^+$ T cells of mice from (G). Data were compared by using one-way analysis of variance (ANOVA) and post hoc Tukey's test in (A) to (C), (F), and (I) or by unpaired two-tailed Student's t test in (H) and (J). Mean fluorescence intensity (MFI) of bulk CD4 T cells of control groups from (H) and (J) are depicted to show baseline expression levels. Error bars indicate mean ± SD. *$P \leq 0.05$; **$P \leq 0.01$; ***$P \leq 0.001$; ****$P \leq 0.0001$. LLOD, lower limit of detection.

IL-2 (Fig. 1I and fig. S3), splenic $CD4^+$ T cells from MOG_{35-55} m1Ψ mRNA–treated mice did not secrete these proinflammatory cytokines, even when exposed to very high antigen concentrations. The only measurable factors were low levels of anti-inflammatory and T_H2 type–associated cytokines such as IL-10, IL-5, and IL-13 (fig. S3). The T cell exhaustion markers TIGIT, TIM-3, PD-1, CTLA-4, and LAG-3 were strongly up-regulated on MOG_{35-55} m1Ψ mRNA–expanded $tetramer^+$ T cells (Fig. 1J).

Exposure to m1Ψ mRNA does not impair the capability to mount immune responses

$CD11c^+$ APCs of mice first exposed to m1Ψ mRNA and thereafter injected with U mRNA did not show any impairment in their ability to respond to this TLR-agonistic stimulus with up-regulation of costimulatory molecules and IFN-α secretion (Fig. 2, A and B). To investigate whether the induction and expansion of MOG_{35-55}–specific $CD4^+$ T_{reg} cells affects de novo priming of antigen-specific immune responses, we exploited two broadly used model systems. First, C57BL/6 mice underwent prime-boost (days 6 and 13) vaccination with U mRNA encoding the ovalbumin (OVA) epitope SIINFEKL and were concurrently exposed to MOG_{35-55}–encoding m1Ψ mRNA (days 0, 3, 7, and 10). SIINFEKL-specific $CD8^+$ T cells were expanded above 40% of total blood $CD8^+$ T cells (Fig. 2C) and displayed properties of effector T (T_{eff}) cells such as cognate IFN-γ secretion and highly potent and antigen-specific killing (Fig. 2, D and E), which suggested uncompromised T cell priming and expansion. In a second experiment, mice were immunized intramuscularly with a self-amplifying RNA (saRNA) vaccine encoding influenza hemagglutinin (HA) (day 6) concurrent to repeated treatment with MOG_{35-55} m1Ψ mRNA or controls. Again, the capability of mice to mount a protective immune response and develop neutralizing antibodies was unimpaired (Fig. 2, F and G). Overall, both studies demonstrate that MOG_{35-55} m1Ψ mRNA–induced antigen-specific $CD4^+$ T_{reg} cells do not suppress functional immune responses against nonmyelin antigens.

Treatment with antigen-encoding m1Ψ mRNA ameliorates EAE in mice

Next, we studied the tolerogenic potential of MOG_{35-55} m1Ψ mRNA in C57BL/6 mice with MOG_{35-55}–induced EAE. Treatment with MOG_{35-55} m1Ψ mRNA was capable of blocking all clinical signs of EAE in mice (Fig. 3A), whereas control animals showed the typical course of the disease with rapid monophasic progression. In mice started on MOG_{35-55} m1Ψ mRNA treatment when a paralysis of the tail or beginning of the hindlimbs were noted (disease score of 1 to 2 of EAE), further disease progression could be prevented, and motor functions were restored (Fig. 3B and fig. S4A). This included occasional cases of reversion of paralysis, which was most likely attributable to an anti-inflammatory effect rather than tissue repair.

Various effects were observed in mice treated with antigen-encoding m1Ψ mRNA compared with control animals. In the brain and spinal cord, the total amount of infiltrating $CD4^+$ T cells, MOG_{35-55}–specific $CD4^+$ T cells and subsets of $CD4^+$ T cells secreting IFN-γ and IL-17A were considerably lower (Fig. 3, C, D, and F, and figs. S4B and S5). Demyelination of the spinal cord was also considerably reduced (Fig. 3E). In the spleen of MOG_{35-55} m1Ψ mRNA–treated animals, we observed an increase of lymphocytes (fig. S5), including MOG_{35-55}–specific $CD4^+$ T cells with low CD62L, CCR6, and CCR7 expression, and up-regulation of CD69 (fig. S6). CCR6, CCR7, and CD62L are critical for access of T cells to the central nervous system (CNS) (*9*–*12*), and the transmembrane C-type lectin CD69 is known to promote lymphocyte retention in the spleen (*13*).

Next, we analyzed the autoantigen-specific $CD4^+$ T cells in those mice in which the manifestation of EAE was prevented by treatment with MOG_{35-55} m1Ψ mRNA on days 7 and 10. MOG_{35-55}–specific splenic $CD4^+$ T cells from treated animals showed down-regulation of the activation marker CD44 and strong expression of coinhibitory molecules (Fig. 3G). At the peak of disease (day 16 after disease induction), CD5, ICOS, LAG-3, PD-1, CTLA-4, TIGIT, and TIM-3 were up-regulated in $tetramer^+$ splenic $CD4^+$ T cells. Furthermore, we detected a highly activated T_{reg} cell population (Fig. 3, H and I) and lower numbers of T_H1 and T_H17 MOG_{35-55}–specific $CD4^+$ T cells (Fig. 3H). Similar findings in mice with symptomatic EAE (disease score of 1 to 2 at start of treatment) further confirmed the potent disease-suppressive activity of antigen-encoding m1Ψ mRNA (fig. S4).

We extended our study of the preventive and therapeutic effect of m1Ψ mRNA to other EAE mouse models. The SJL model is based on autoreactivity against the $PLP_{139-151}$ epitope and is characterized by recurring EAE symptoms resulting in a relapsing-remitting disease, similar to the clinical presentation of MS in patients. Treatment of SJL mice with $PLP_{139-151}$ m1Ψ mRNA twice a week starting from day 7 after EAE induction resulted in almost full disease control (fig. S7A). Even when the mice were treated after the first disease peak (starting on day 14 after disease induction), progression of the disease was halted (fig. S7B).

Treatment with m1Ψ mRNA leads to therapeutically effective bystander tolerance

In another experimental setup, we addressed a key challenge in human MS, namely that antigen spread leads to a complex antimyelin autoreactivity pattern and the specificity of autoreactive T cell clones in individual patients, and thus, the potential targets for direct antigen-specific tolerization is unknown. A clinically viable approach would be to use bystander tolerance by inducing T_{reg} cells, which, once activated by their cognate antigen, would suppress T cells against other antigens in the inflamed tissue.

We evaluated bystander activity in two experimental settings. F1 C57BL/6 x SJL mice with $PLP_{139-151}$ peptide–induced EAE were vaccinated with m1Ψ mRNA encoding either $PLP_{139-151}$ (the disease-causing autoantigen), MOG_{35-55} (unrelated autoantigen, against which m1Ψ mRNA is capable of inducing potent effector T_{reg} cells), or irrelevant m1Ψ mRNA (Fig. 4A and fig. S7C). MOG_{35-55} m1Ψ mRNA treatment showed a dose-dependent therapeutic effect on EAE, similar to the curative effect mediated by vaccination with $PLP_{139-151}$ m1Ψ mRNA, indicating a strong T_{reg} cell–mediated bystander suppression, also given the fact that antigen spread has been described for this particular EAE model (*14*). Antigen-specific T_{reg} cells were notably expanded and highly activated, constituting >80% of de novo expanded MOG_{35-55}–specific $CD4^+$ splenic T cells (Fig. 4, B and C). T_{eff} cell infiltration into the brain and spinal cord in m1Ψ mRNA–treated mice was reduced (Fig. 4, D to F), and no signs of demyelination in the spinal cord were detected (Fig. 4G).

We also investigated a complex EAE model driven by multiple pathogenic autoreactive T cell clones against MOG_{35-55}, $PLP_{139-151}$, $PLP_{178-191}$, MBP_{84-104}, and $MOBP_{15-36}$, which could be successfully treated with the mixture of m1Ψ mRNAs coding for the corresponding four disease-inducing autoantigenic epitopes. m1Ψ mRNA encoding MOG_{35-55} were therapeutically almost as effective as those encoding the cocktail of all four disease targets. This suggests that even polyclonal autoimmune disease driven by a broad autoreactive T cell repertoire can be sufficiently controlled by m1Ψ mRNA targeting a strong bystander tolerance–mediating T cell epitope (fig. S7D).

One potential risk associated with antigen-specific tolerization is the induction of autoantibodies against respective targets, which can exacerbate disease (*15*). Moreover, nucleoside-modified mRNA is known to be highly immunogenic and to induce high antibody titers when formulated with immune stimulatory lipid nanoparticles (*16*). We therefore analyzed anti–MOG_{35-55} immunoglobulin G (IgG) antibody responses in the sera of EAE mice upon m1Ψ mRNA vaccination. First, we measured anti–MOG_{35-55} levels in sera of MOG_{35-55} peptide–induced EAE (C57BL/6 mice), which were vaccinated with MOG_{35-55} m1Ψ mRNA on days 7 and 10 after EAE induction. Anti–MOG_{35-55} IgG levels were not elevated in comparison with those of control animals treated

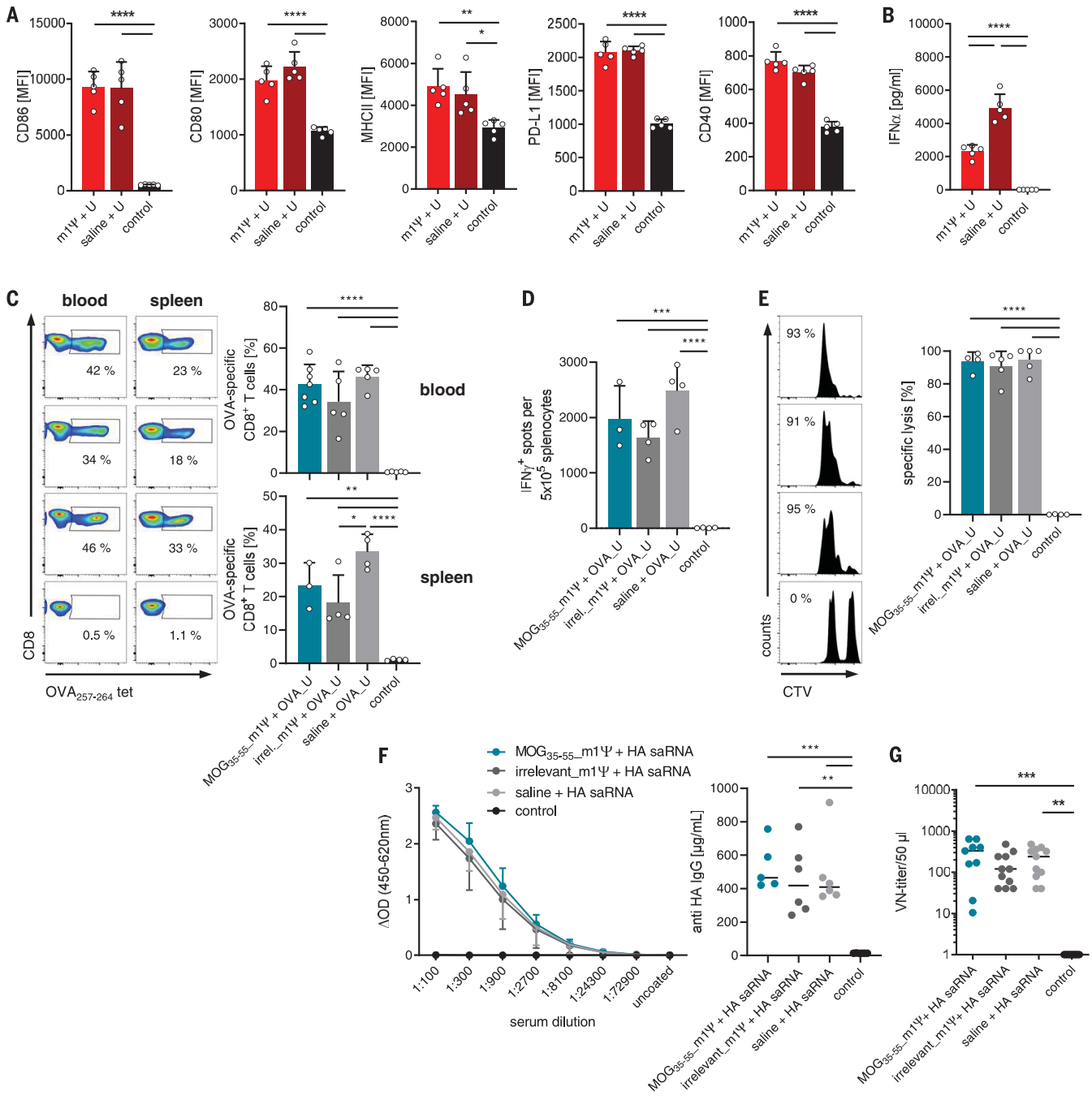

Fig. 2. Exposure to m1Ψ mRNA does not impair the capability to mount immune responses. (**A**) Activation of splenic CD11c$^+$ APCs 24 hours after (n = 3) and (**B**) IFN-α serum levels 6 hours after intravenous injection (day 3) of LPX-formulated U mRNA or saline (control) in C57BL/6 mice (n = 6), which were pretreated with m1Ψ mRNA or saline (control) at day 0. MHCII, major histocompatibility complex II. (**C** to **E**) De novo priming of SIINFEKL-specific CD8$^+$ T cells in C57BL/6 mice with prior exposure to MOG_{35-55} or irrelevant m1Ψ mRNA or saline (days 0, 3, 7, and 10) to SIINFEKL U mRNA prime-boost vaccination (days 6 and 13). Controls only received saline. (C) Frequency of SIINFEKL-specific CD8$^+$ T cells ($OVA_{257-264}$ tet) in blood (n = 5 to 7) and spleen (n = 3 to 4). (D) IFN-γ secretion was measured by ELISpot upon restimulation of total splenocytes of mice from (C) (n = 3 to 4) with SIINFEKL peptide and (E) in vivo antigen-specific killing of adoptively transferred CTV-labeled and peptide-loaded splenocytes of naïve mice (n = 4 to 5). For in vivo cytotoxicity assays, mice were adoptively transferred on day 18 with 0.5 µM (low) or 5 µM (high) CTV-labeled naïve splenocytes pulsed with peptide (6 µg/ml). Of these target cells, 1.5 × 10^6 cells were adoptively transferred into immunized and control recipients at a ratio of 1:1 (irrelevant $HA_{518-526}$ peptide–loaded CTV_{low}:SIINFEKL peptide–loaded CTV_{high}). Recipient splenocytes were recovered and analyzed by flow cytometry 18 hours after transfer, and antigen-specific lysis was determined as follows: specific lysis (%) = [1 − (percentage of cells pulsed with SIINFEKL/percentage of cells pulsed with HA) × 100]. (**F**) Total (n = 5 to 6) and (**G**) neutralizing (n = 9 to 11) anti-HA IgG in C57BL/6 mice with prior exposure to MOG_{35-55} or irrelevant m1Ψ mRNA or saline (days 0, 3, 7, and 10). Controls only received saline. Protective immune responses were measured 28 days after mice were immunized with influenza HA-saRNA (1 µg intramuscularly) on day 6. Data were compared by using one-way ANOVA and post hoc Tukey's test. Error bars, mean ± SD. ΔOD, change in optical density; VN, virus neutralizing.

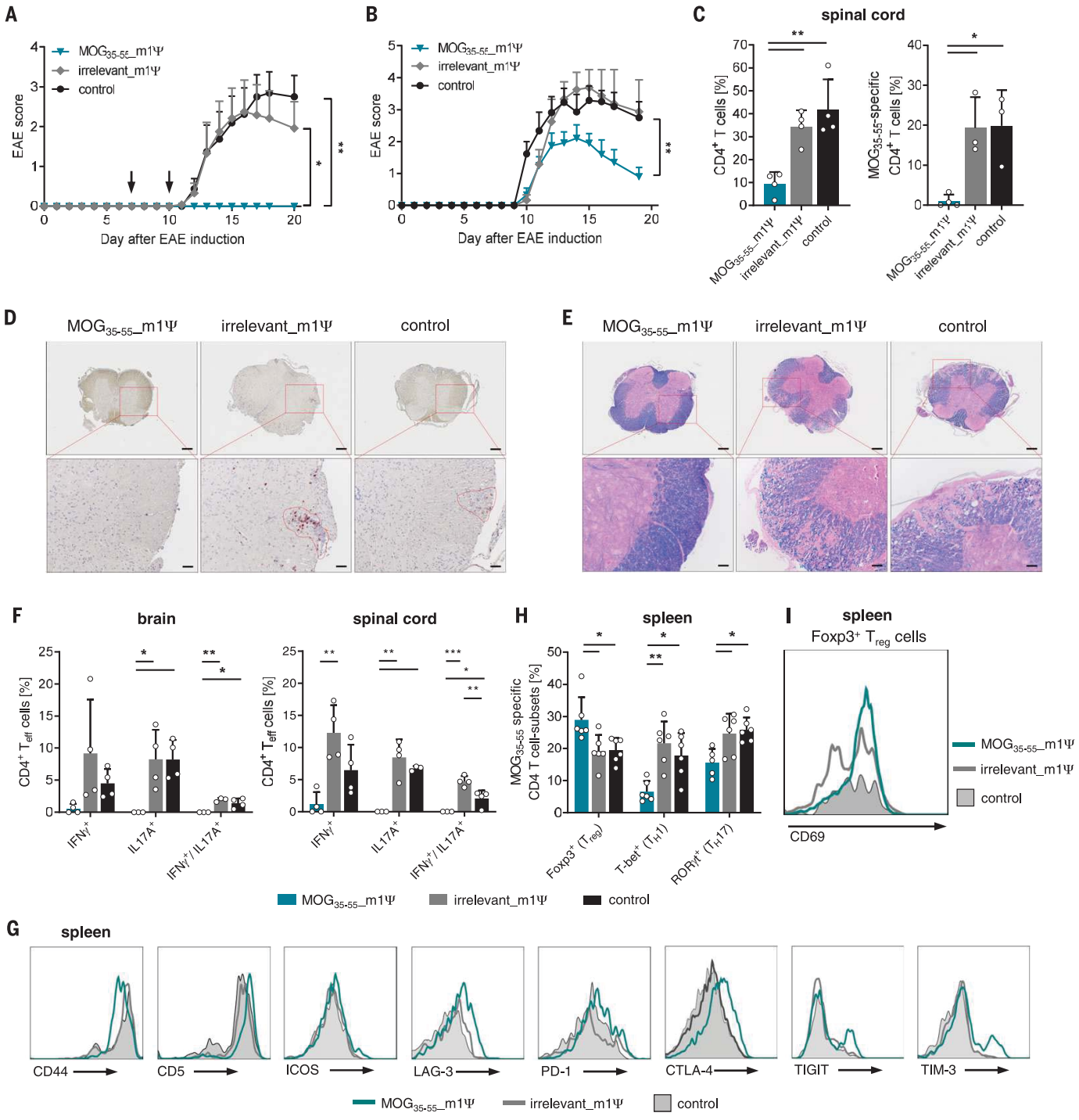

Fig. 3. Treatment with antigen-encoding m1Ψ mRNA ameliorates EAE in mice. (**A** and **B**) Disease severity in MOG_{35-55}–induced EAE (n = 6 to 8 C57BL/6 mice per group) treated with m1Ψ mRNA or saline (control) (A) on days 7 and 10 after disease induction or (B) when disease progressed to a score of 1 to 2. (**C**) Frequency of $CD4^+$ T cell and MOG_{35-55}–specific $CD4^+$ T cells in the spinal cord of mice treated on days 7 and 10 after disease induction (n = 3 to 4). $Thy1.1^+$ 2D2 $CD4^+$ T cells were transferred 1 day before EAE induction into $Thy1.2^+$ recipient mice and analyzed in the target organs on day 16 after disease induction. (**D**) Representative CD4 staining in the spinal cord of EAE mice treated with m1Ψ mRNAs or saline (control) (n = 3) on days 7 and 10 after disease induction and analyzed at day 16 after EAE induction. (**E**) Representative Luxol fast blue (LFB) staining revealing areas of demyelination in the spinal cord of mice from (D) (n = 3). (**F** to **I**) Frequency of $CD4^+$ IFN-γ– and IL-17A–secreting cells in brain and spinal cord (n = 3 to 4) (F) and flow cytometry analysis of splenic tetramer$^+$ $CD4^+$ T cells (n = 4 to 6) [(G) to (I)] of EAE mice treated with m1Ψ mRNAs or saline (control) on days 7 and 10 after disease induction and analyzed at day 16 after EAE induction. Area under the curve (AUC) was used to determine statistical significance through one-way ANOVA and Tukey's multiple comparison test of the different EAE disease development curves in (A) and (B). Data were compared by using one-way ANOVA and post hoc Tukey's test in (F) and (H). Error bars indicate mean ± SEM in (A) and (B) or mean ± SD in (C), (F), and (H). The scale bar in the upper row of (D) and (E) represents 200 μm and, in the lower row of (D) and (E), represents 50 μm.

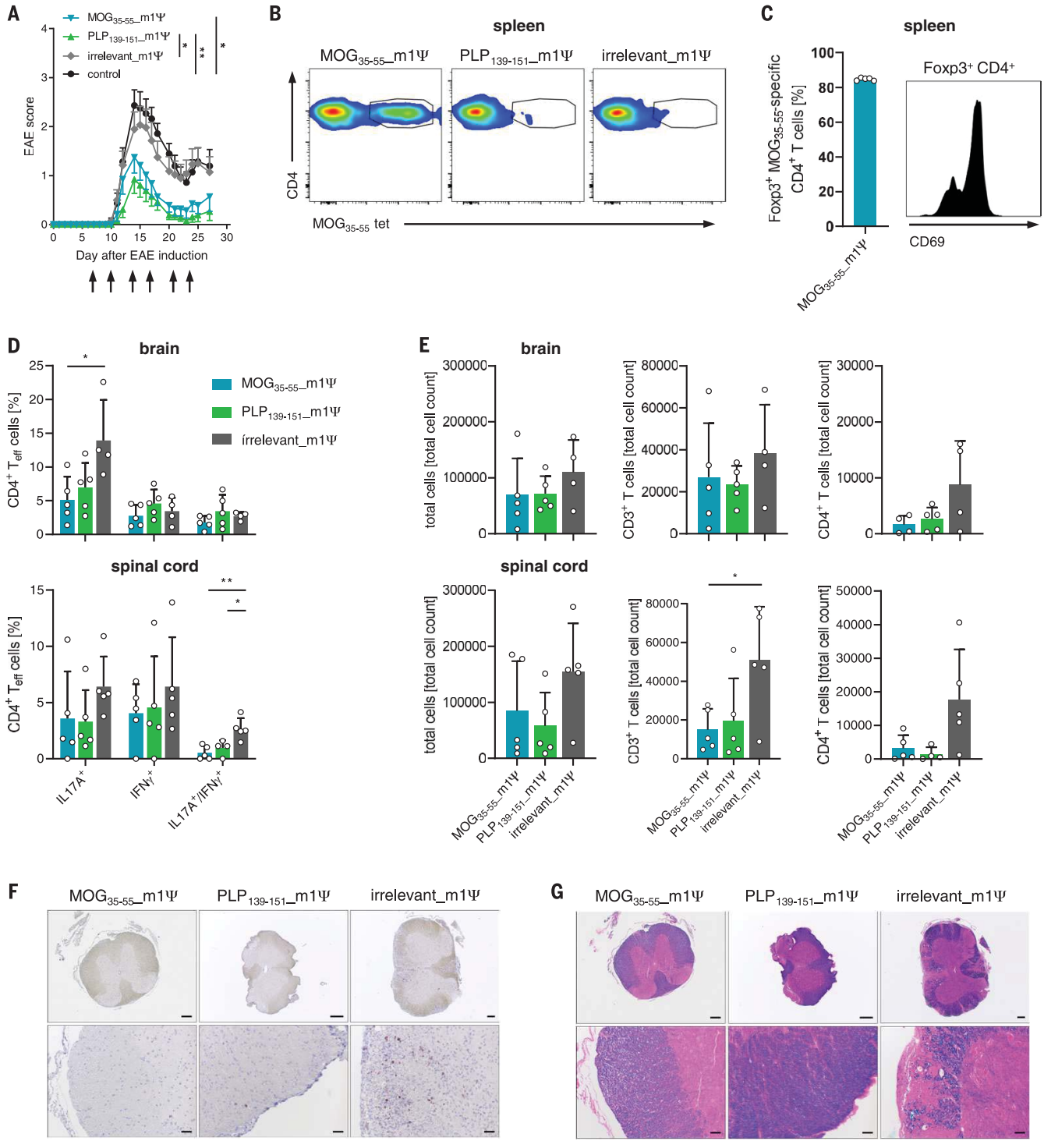

Fig. 4. Treatment with m1Ψ mRNA leads to therapeutically effective bystander tolerance. (**A**) Dynamics of EAE in $PLP_{139-151}$–induced EAE mice (n = 13 to 15 F1 C57BL/6 x SJL mice) upon treatment with MOG_{35-55} m1Ψ, $PLP_{139-151}$ m1Ψ, irrelevant m1Ψ mRNA, or saline (control) twice per week starting on days 7 and 10 after disease induction with 40 μg of m1Ψ mRNA. (**B** and **C**) Expansion of endogenous MOG_{35-55}–specific $CD4^+$ T cells (B) and frequency of $Tetramer^+$ $Foxp3^+$ T_{reg} cells and analysis of CD69 expression on respective cell population (C) upon treatment with m1Ψ mRNA measured in the spleen on day 28 after EAE induction (n = 5). (**D**) Frequency of $CD4^+$ IFN-γ– and IL-17A–secreting cells upon $PLP_{139-151}$–peptide restimulation and (**E**) total cell count of lymphocytes in brain and spinal cord of EAE mice treated with different m1Ψ mRNAs (n = 4 to 5) and analyzed on day 28 after EAE induction. (**F**) Representative CD4 staining in the spinal cord of EAE mice from (A) (n = 2). (**G**) Representative LFB staining revealing areas of demyelination in the spinal cord of mice from (A) (n = 2). AUC was used to determine statistical significance through one-way ANOVA and Tukey's multiple comparison test of the different EAE disease development curves (A). Data were compared by using one-way ANOVA and post hoc Tukey's test. Error bars indicate mean ± SEM in (A) or mean ± SD in (C) to (E). The scale bar in the upper row of (F) and (G) represents 200 μm and, in the lower row of (F) and (G), represents 50 μm.

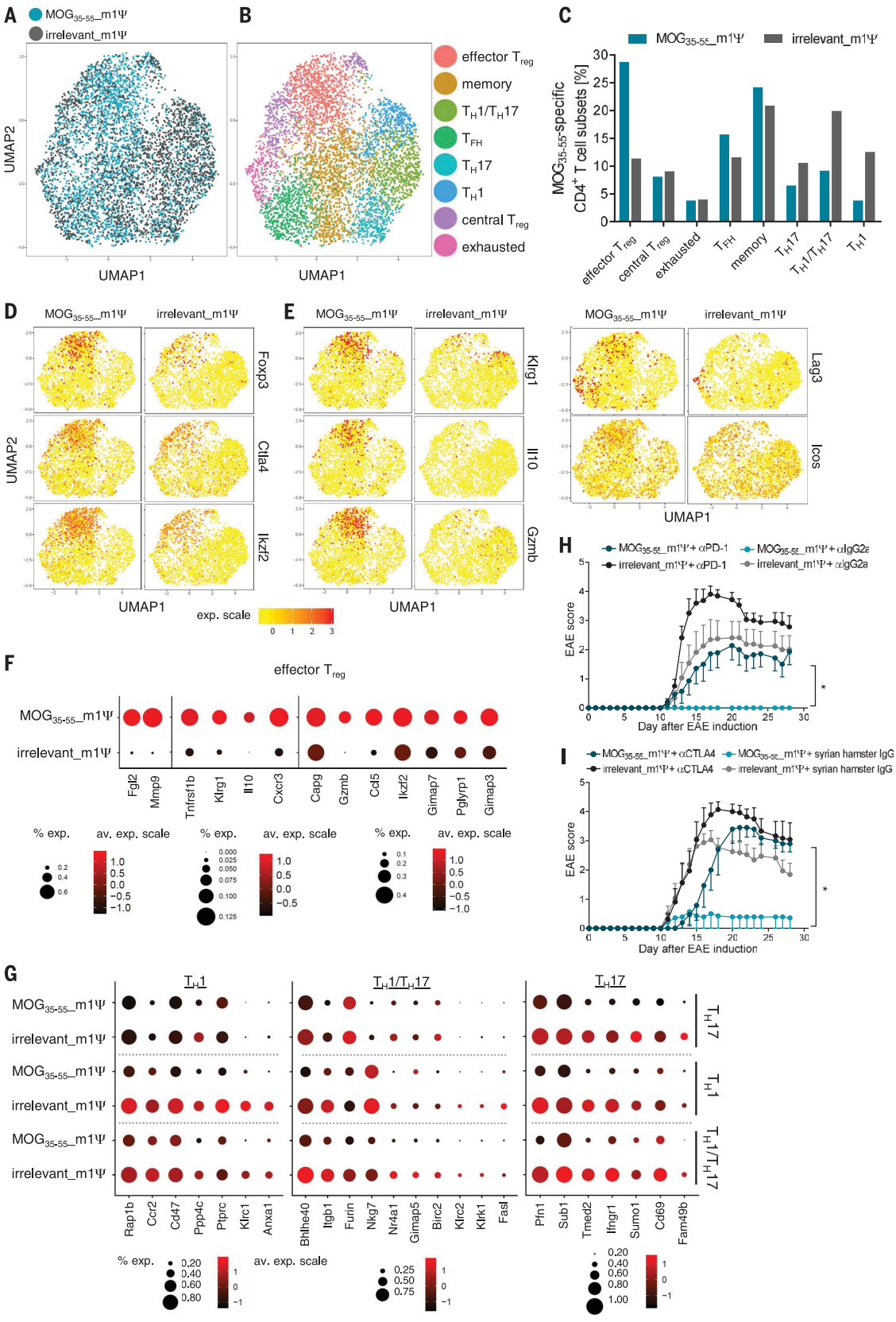

Fig. 5. Distinct splenic antigen-specific CD4$^+$ T cell subsets are expanded in EAE mice treated with antigen-encoding m1Ψ mRNA. (**A** to **G**) MOG_{35-55}–specific CD4$^+$ T cells isolated from mice with MOG_{35-55}–induced EAE treated with m1Ψ mRNA on days 7 and 10 after disease induction and analyzed by single-cell RNA sequencing on day 15 or day 16, respectively. (A) A two-dimensional uniform manifold approximation and projection (UMAP) projection of MOG_{35-55}–specific CD4$^+$ T cells isolated from different treatment groups (each dot represents one cell) identified by unsupervised clustering. (B) UMAP projection of single cells, color-coded according to the identified cell subsets. (C) Frequency of different cell subsets. (D) and (E) depict a UMAP projection of classical T_{reg} cell markers (D) and effector T_{reg} cell markers (E). (F) Genes up-regulated in an effector T_{reg} subpopulation upon MOG_{35-55} m1Ψ mRNA treatment (adjusted P value < 0.05). av. exp., average expression. (G) Genes down-regulated upon MOG_{35-55} m1Ψ mRNA treatment in T_H1, T_H17, and T_H1/T_H17 cell subsets (adjusted P value < 0.05). (**H** and **I**) MOG_{35-55}–induced EAE in C57BL/6 mice (n = 8 per group) treated with m1Ψ mRNA on days 7 and 10 after disease induction in combination with (H), anti–PD-1, and (I) anti–CTLA-4 blocking antibodies or isotype controls administered twice per week. Statistical significance of AUC differences of EAE disease development curves was assessed by using one-way ANOVA and Tukey's multiple comparison test in (H) and (I). Error bars represent mean ± SEM in (H) and (I).

with irrelevant m1Ψ mRNA or saline (fig. S8A). This suggests that m1Ψ mRNA application does not exacerbate preformed autoantibody responses. Even after repetitive MOG_{35-55} m1Ψ mRNA challenge (twice per week, 12 times in total) of F1 C57BL/6 x SJL mice, no anti–MOG_{35-55} IgG antibodies were detected in those where EAE was induced with $PLP_{139-151}$–peptide immunization (fig. S8B).

Distinct antigen-specific CD4$^+$ T cell subsets are expanded in EAE mice treated with antigen-encoding m1Ψ mRNA

Next, we characterized the tolerized T cells by subjecting splenic tetramer$^+$ CD4$^+$ T cells from animals treated with MOG_{35-55} m1Ψ mRNA or irrelevant m1Ψ mRNA to single-cell RNA sequencing (table S1). Clustering analysis revealed eight distinct antigen-specific CD4$^+$ T cell subsets in EAE mice (Fig. 5, A and B, and fig. S9). The CD4$^+$ T cell identity of all subsets was confirmed with canonical T cell markers (fig. S10). We used sets of genes characterizing different functional T cell subphenotypes for further analysis (figs. S11 and S12). We identified two distinct populations sharing common T_{reg} cell markers (*Foxp3*, *Ikzf2*, and *Ctla4*). One of these subpopulations displayed typical effector T_{reg} cell markers (*Klrg1*, *Il10*, *Gzmb*, *Lag3*, and *Icos*), whereas the other subset were central T_{reg} cells as defined by markers *Sell* and *Bcl2* and low expression of the common effector-associated molecules (*17*, *18*) (figs. S11, A and B, and S13A). We also identified T_H1 (*Ifnγ* and *Tbx21*), T_H17 (*Il17a/f* and *Tmem176a/b*), and T_H1/T_H17 cells with combined expression of T_H1 and T_H17 markers (*Csf2*, *Tbx21*, *Ifnγ*, and *Il17a*). Moreover, we found exhausted antigen-specific T cells (*Lag3* and *Cd160*), T follicular helper (T_{FH}) cells (*Il4*, *Il21*, and *Cxcr5*), and a T cell cluster with a memory phenotype (*Ccr7*^{high} and *Tcf7*^{high}) (figs. S11, C to H, and S13, B and C).

The relative frequencies of these antigen-specific CD4$^+$ T cell subpopulations changed in EAE mice treated with antigen-encoding m1Ψ mRNA. Most notably, in animals treated with MOG_{35-55} m1Ψ mRNA, the effector T_{reg} cells constituted the largest cluster by frequency and cell count (Fig. 5C). The T_H1, T_H17, and T_H1/T_H17 T_{eff} cell subpopulations were strongly reduced in comparison with those of control animals treated with irrelevant m1Ψ mRNA, whereas exhausted T cell and central T_{reg} cell subpopulations were of similar size in both groups (Fig. 5C). We also found substantial differences in the expression levels of functionally relevant genes and activation markers. Common T_{reg} cell markers such as *Foxp3*, *Ikzf2*, and *Ctla4* were present in T_{reg} cell subpopulations of both treatment groups (Fig. 5D), whereas transcripts characteristic for effector T_{reg} cells and associated with T_{reg} cell suppressive function, such as *Klrg1*, *Il10*, *Gzmb*, *Lag3*, and *Icos*, were enriched in MOG_{35-55} m1Ψ mRNA–treated EAE mice and almost completely absent in those treated with irrelevant m1Ψ mRNA (Fig. 5, E and F). Likewise, the transcript profiles of the T_H1, T_H17, and T_H1/T_H17 T_{eff} cell clusters differed considerably between the two treatment groups (Fig. 5G and fig. S14A). The most prominent examples of differentially regulated genes were those involved in differentiation (*Anxa1*, *Ppp4c*, and *Mid1*) (*19*–*21*), migration (*Ccr2*, *Itgb1*, *Wdr26*, and *Rap1b*) (*22*–*26*) or cytokine production of T_{eff} cells (*Bhlhe40*) (*27*). In accordance with a previous study (*28*), we detected mainly down-regulation of genes associated with cell cycle and cell division in the mice treated with MOG_{35-55} m1Ψ mRNA (fig. S14B). The number of genes up-regulated in T_H1, T_H17, and T_H1/T_H17 T_{eff} cell subpopulations from MOG_{35-55} m1Ψ mRNA–treated mice was small (fig. S14A).

To visualize the relationships between the identified major cell populations, we performed single-cell trajectory analysis (fig. S15). Each state represents subpopulation structures of closely related transitory cellular states. T cells from mice treated with irrelevant m1Ψ mRNA appeared mainly as fully differentiated cells in state 5, representing T_H1, T_H17, and T_H1/T_H17 T_{eff} cells (fig. S15, B, D, and F). By contrast, T cells from the MOG_{35-55} m1Ψ mRNA–treated group were in state 1 (memory) or mainly differentiated in state 2, representing effector T_{reg} cells and T_{FH} cells (fig. S15, B, C, and F). In sum, these findings indicate that m1Ψ mRNA treatment rather than deleting autoreactive T cells tips the immunological balance in favor of suppression of disease promoting MOG_{35-55}–specific T_H1, T_H17, and T_H1/T_H17 T_{eff} cells by expanding effector T_{reg} cells.

PD-1 and CTLA-4 signaling contribute to the induction and maintenance of antigen-specific tolerance

Expression of coinhibitory receptors such as CTLA-4 and PD-1 on effector and T_{reg} cells is a key mechanism of immune homeostasis. We therefore assessed the mechanistic contribution of these pathways to antigen-specific tolerance mediated by m1Ψ mRNA. Treatment of EAE mice with MOG_{35-55} m1Ψ mRNA combined with anti–PD-1 or anti–CTLA-4 antibody on days 7 and 10 after EAE induction aggravated the disease in control groups in accordance with the known unleashing effect of checkpoint blockade on autoreactive T cells (*29*). Both CTLA-4 and PD-1 blockade almost completely abolished the EAE-protective effect of MOG_{35-55} m1Ψ mRNA (Fig. 5, H and I). Flow cytometry and single-cell RNA sequencing revealed almost exclusive and high expression of *Ctla4* by MOG_{35-55}–specific CD4$^+$ T_{reg} cells (fig. S16, A and B), which supports a role of this population for mediating tolerance. The effect of PD-1 blockade may be driven by two independent mechanisms, one being invigoration of preexistent T_{eff} cells and the other being the inhibition of the de novo induction of antigen-specific T_{reg} cells, which also depends crucially on PD-1 signaling (*30*). These findings suggest that disease-mediating T cells are suppressed but not deleted in mice treated with antigen-encoding m1Ψ mRNA and that both PD-1 and CTLA-4 signaling critically contribute to the induction and maintenance of antigen-specific tolerance.

Discussion

Our study describes nanoparticulate delivery of nucleoside-modified autoantigen-encoding mRNA into lymphoid CD11c$^+$ APCs as a therapeutic approach for antigen-specific tolerization. We show, at single-cell resolution, the generation of different antigen-specific CD4$^+$ T cell subpopulations with distinct functional states.

Selective delivery of autoantigens into CD11c$^+$ APCs resident in lymphoid tissues exploits a highly effective natural mechanism for induction and maintenance of peripheral tolerance. The presentation of autoantigens in a noninflammatory context leads to expansion of antigen-specific CTLA-4$^+$, ICOS$^+$, IL-10$^+$, and Foxp3$^+$ effector T_{reg} cells (*31*) that not only suppress antigen-specific autoreactive T_{eff} cells but also exert bystander immunosuppression, thereby enabling disease control even in a complex, polyclonal model of autoimmunity.

Bystander activity of T_{reg} cells has been associated with noncognate mechanisms depending on cell-cell interaction, such as secretion of suppressive factors, e.g., IL-10 and transforming growth factor–β (TGF-β) (*32*). Thus, one would expect that MOG-specific T_{reg} cells activated upon reexposure to their cognate antigen in the CNS would suppress immune responses that occur at that very location for a defined period of time. Because of its temporo-spatial nature, T_{reg} cell activity exerts tissue-specific immune regulation rather than pan-immune suppression (*33*). This is in line with prior studies indicating that T cell tolerance to tissue-restricted self-antigens is actively mediated by antigen-specific T_{reg} cells rather than deletion (*34*).

With the presented approach, key challenges for clinical translation of antigen-based treatment of autoimmune diseases can be addressed. Both the nucleoside-modified, purified mRNA and the liposomal nanoparticle formulation are pharmaceutically well-defined clinical-stage compounds and are currently being explored in human trials for various disease indications (*35*). The repetitive administration of m1Ψ mRNA is not compromised by induction of autoantigen-specific antibody responses, which usually causes safety-limiting constraints for other applications. Production of mRNA pharmaceuticals is fast and cost-efficient, and virtually any autoantigen can be encoded by

mRNA. Thus, tailoring the treatment for the disease-causing antigens of individual patients is conceivable, similar to that which has been successfully executed in the setting of personalized cancer vaccines (*36*, *37*). Combination of m1Ψ mRNAs encoding either multiple personalized autoantigens or autoantigens that confer bystander tolerance may enable control of even complex autoimmune diseases.

REFERENCES AND NOTES

1. P. Serra, P. Santamaria, *Nat. Biotechnol.* **37**, 238–251 (2019).
2. A. Miller, O. Lider, H. L. Weiner, *J. Exp. Med.* **174**, 791–798 (1991).
3. L. M. Kranz *et al.*, *Nature* **534**, 396–401 (2016).
4. K. Karikó, M. Buckstein, H. Ni, D. Weissman, *Immunity* **23**, 165–175 (2005).
5. K. Karikó *et al.*, *Mol. Ther.* **16**, 1833–1840 (2008).
6. K. Karikó, H. Muramatsu, J. Ludwig, D. Weissman, *Nucleic Acids Res.* **39**, e142 (2011).
7. N. Yogev *et al.*, *Immunity* **37**, 264–275 (2012).
8. E. Bettelli *et al.*, *J. Exp. Med.* **197**, 1073–1081 (2003).
9. I. S. Grewal *et al.*, *Immunity* **14**, 291–302 (2001).
10. Y. Arima *et al.*, *Cell* **148**, 447–457 (2012).
11. A. Reboldi *et al.*, *Nat. Immunol.* **10**, 514–523 (2009).
12. S. Noor, E. H. Wilson, *J. Neuroinflammation* **9**, 77 (2012).
13. L. R. Shiow *et al.*, *Nature* **440**, 540–544 (2006).
14. R. Gold, C. Linington, H. Lassmann, *Brain* **129**, 1953–1971 (2006).
15. C. P. Genain *et al.*, *Science* **274**, 2054–2057 (1996).
16. N. Pardi *et al.*, *Nat. Commun.* **9**, 3361 (2018).
17. E. Cretney, A. Kallies, S. L. Nutt, *Trends Immunol.* **34**, 74–80 (2013).
18. R. J. Miragaia *et al.*, *Immunity* **50**, 493–504.e7 (2019).
19. N. Paschalidis *et al.*, *J. Neuroinflammation* **6**, 33 (2009).
20. S. A. Apostolidis, T. Rauen, C. M. Hedrich, G. C. Tsokos, J. C. Crispín, *J. Biol. Chem.* **288**, 26775–26784 (2013).
21. A. Collison *et al.*, *Nat. Med.* **19**, 232–237 (2013).
22. E. E. Kara *et al.*, *Nat. Commun.* **6**, 8644 (2015).
23. B. T. Fife, G. B. Huffnagle, W. A. Kuziel, W. J. Karpus, *J. Exp. Med.* **192**, 899–906 (2000).
24. S. Glatigny, R. Duhen, M. Oukka, E. Bettelli, *J. Immunol.* **187**, 6176–6179 (2011).
25. C. Runne, S. Chen, *Cell Adh. Migr.* **7**, 214–218 (2013).
26. T. Kinashi, K. Katagiri, *Immunol. Lett.* **93**, 1–5 (2004).
27. C. C. Lin *et al.*, *Nat. Commun.* **5**, 3551 (2014).
28. B. R. Burton *et al.*, *Nat. Commun.* **5**, 4741 (2014).
29. L. M. Yshii, R. Hohlfeld, R. S. Liblau, *Nat. Rev. Neurol.* **13**, 755–763 (2017).
30. L. Wang *et al.*, *Proc. Natl. Acad. Sci. U.S.A.* **105**, 9331–9336 (2008).
31. N. Ohkura, S. Sakaguchi, *Nat. Immunol.* **12**, 283–284 (2011).
32. A. M. Thornton, E. M. Shevach, *J. Immunol.* **164**, 183–190 (2000).
33. X. Clemente-Casares *et al.*, *Nature* **530**, 434–440 (2016).
34. F. P. Legoux *et al.*, *Immunity* **43**, 896–908 (2015).
35. N. Dammes, D. Peer, *Trends Pharmacol. Sci.* **41**, 755–775 (2020).
36. U. Sahin, Ö. Türeci, *Science* **359**, 1355–1360 (2018).
37. U. Sahin *et al.*, *Nature* **547**, 222–226 (2017).

ACKNOWLEDGMENTS

We thank V. Ames, K. Zwadlo, A. Plaschke, I. Beulshausen, E. Petscherskich, E. Daniel, R. Roth, B. Jesionek, M. Brkic, A. Selmi, M. Baiersdörfer, and S. Berl for technical assistance; S. Witzel, B. Tillmann, S. Wurzel, Z. Yildiz, and N. Blaumeuser for cloning of constructs; S. Fesser, K. Tillmann, J. Beckerle, E. Heintz, and C. Golletz for mRNA production; and P. Guna, A.-L. Popa, and H. Haas for providing liposomes. Additional support was provided by S. Attig and A. Hohberger for cell sorting. Moreover, we acknowledge F. Vascotto for support and scientific discussion for the manuscript, T. Regen for experimental advice, and L. Giese for supporting single-cell RNA sequencing. Furthermore, we thank the NIH Tetramer Core Facility for providing the MOG_{35-55} MHC class II tetramer. **Funding:** This work has been supported by grants from the Immunology Research Center (FZI) Mainz (FZI-TRP 2014-12 to U.S. and N.Y.) and the Deutsche Forschungsgemeinschaft DFG (SFB/CRC-TR 128 to A.W.). **Author contributions:** U.S. was responsible for conception and experimental strategy of the study. Planning and analysis of the experiments were done by C.K., L.M.K., M.D., S.Kr., H.B., and J.P., supported by N.Y. and A.W. C.K. and S.Ki. performed immunological experiments. Processing and analysis of scRNA-seq data was done by L.K., E.D., and M.S., supported by T.B. Ö.A.-Ö. performed IHC experiments. C.K., Ö.T., and U.S. interpreted the data and drafted the manuscript. L.K., E.D., M.S., M.D., K.K., and A.W. supported writing of the manuscript. All authors edited and approved the final manuscript. **Competing interests:** L.M.K., H.B., K.K., Ö.T., and U.S. are employees at BioNTech SE (Mainz, Germany). M.D. and S.Kr. work as consultants for BioNTech SE (Mainz, Germany). C.K., J.P., L.M.K., M.D., S.Kr., K.K., and U.S. are inventors on patents and patent applications related to this study. Ö.T. and U.S. are stock owner and management board members of BioNTech SE (Mainz, Germany). All other authors declare no competing interests. **Data and materials availability:** Correspondence and request for materials should be addressed to U.S.

SUPPLEMENTARY MATERIALS

science.sciencemag.org/content/371/6525/145/suppl/DC1
Materials and Methods
Figs. S1 to S16
Tables S1 and S2
References (*38*–*52*)

View/request a protocol for this paper from *Bio-protocol*.

13 June 2019; resubmitted 27 April 2020
Accepted 17 November 2020
10.1126/science.aay3638

A noninflammatory mRNA vaccine for treatment of experimental autoimmune encephalomyelitis

Christina Krienke, Laura Kolb, Elif Diken, Michael Streuber, Sarah Kirchhoff, Thomas Bukur, Özlem Akilli-Öztürk, Lena M. Kranz, Hendrik Berger, Jutta Petschenka, Mustafa Diken, Sebastian Kreiter, Nir Yogev, Ari Waisman, Katalin Karikó, Özlem Türeci and Ugur Sahin

Science **371** (6525), 145-153.
DOI: 10.1126/science.aay3638

Precision therapy for immune tolerance

Autoimmune diseases, such as multiple sclerosis (MS), result from a breach of immunological self-tolerance and tissue damage by autoreactive T lymphocytes. Current treatments can cause systemic immune suppression and side effects such as increased risk of infections. Krienke *et al.* designed a messenger RNA vaccine strategy that lacks adjuvant activity and delivers MS autoantigens into lymphoid dendritic cells. This approach expands a distinct type of antigen-specific effector regulatory T cell that suppresses autoreactivity against targeted autoantigens and promotes bystander suppression of autoreactive T cells against other myelin-specific autoantigens. In mouse models of MS, the vaccine delayed the onset and reduced the severity of established disease without showing overt symptoms of general immune suppression.

Science, this issue p. 145

Supplementary Materials for

A noninflammatory mRNA vaccine for treatment of experimental autoimmune encephalomyelitis

Christina Krienke, Laura Kolb*, Elif Diken*, Michael Streuber, Sarah Kirchhoff, Thomas Bukur, Özlem Akilli-Öztürk, Lena M. Kranz, Hendrik Berger, Jutta Petschenka, Mustafa Diken, Sebastian Kreiter, Nir Yogev, Ari Waisman, Katalin Karikó, Özlem Türeci, Ugur Sahin†

*These authors contributed equally to this work.
†Corresponding author. Email: sahin@uni-mainz.de

Published 8 January 2021, *Science* **371**, 145 (2021)
DOI: 10.1126/science.aay3638

This PDF file includes:

MATERIALS AND METHODS

Mice. C57BL/6, albino C57BL/6, SJL/JRj wild-type mice and F1 hybrid mice from C57BL/6 and SJL/JRj were purchased from ENVIGO RMS GmbH, Netherlands and Janvier Laboratories, France, respectively. Thy1.1$^+$ 2D2 TCR-transgenic C57BL/6 and Thy1.1$^+$ 2D2 Foxp3-eGFP TCR-transgenic C57BL/6 mice were provided by Ari Waisman. Age and sex matched animals were used throughout the experiments and mice were maintained under specific pathogen-free (SPF) conditions at the animal facility of BioNTech SE Mainz. All animal experiments were performed in accordance with federal and state policies.

RNA constructs and *in vitro* transcription. All sequences corresponding to mRNAs were cloned into the multiple-cloning site (MCS) of pST1-hAg-MCS-FI-A30LA70 plasmid. The plasmid-backbone contained sequences corresponding to: human alpha globin 5'UTR (hAg), a 3' UTR of FI element and a poly(A) tail of 100 nucleotides, interrupted by a short linker after 30 nucleotides (A30LA70, L = GCAUAUGACU). The coding sequences of all antigen-encoding templates (MOG_{35-55}, $PLP_{139-151}$, $PLP_{178-191}$ and MBP_{84-104}, $OVA_{257-264}$ (SIINFEKL) constructs) were fused to an upstream mmsec and downstream mmMITD sequence (pST1-hAg-mmsec(opt)-MCS-mmMITD(opt)-A30LA70), respectively, as the addition of a leader peptide and an MHC trafficking signal (MITD) strongly improves antigen presentation by APCs (*38*). In all myelin-derived antigen-sequences the disease relevant epitope was flanked by seven amino acids to facilitate antigen presentation. The resulting peptide-sequences were: MOG_{27-63}: SPG KNA TGM EVG WYR SPFS RVV HLY RNG KDQ DAE AQP, $PLP_{131-159}$: AHS LER VCH CLG KWL GHP DKF VGI TYA LT, $PLP_{170-199}$: AVP VYI YFN TWT TCQ SIA FPS KTS ASI GSL and MBP_{76-112}: RTQ DEN PVV HFF KNI VTP RTP PPS QGK GRG LSL SRF. For control immunization with irrelevant mRNA, empty vector was used, coding for no specific antigen-sequence (pST2-hAg-mmsec(opt)-empty-mmMITD(opt)-2hBg-A30LA70). The plasmid vector constructs encoding firefly luciferase (LUC) were cloned into the pST1-hAg-CDS-FI-A30LA70 plasmid-backbone. Linearization of plasmids, and *in vitro* transcription of mRNA were conducted as described previously (*38*). Influenza-Hemagglutinin (HA)-encoding self-amplifying RNA (saRNA) was designed as previously described (*39*).

Generation of non-immunogenic mRNA. For *in vitro* transcription of mRNA from the DNA template, 1-methylpseudouridine-5'-triphosphate (m1ΨTP) (TriLink) was used instead of uridine-5'-triphosphate (UTP), and mRNA was purified by HPLC or cellulose (*40*). For HPLC purification the protocol of Weissman et al., 2013 (*41*), was adapted and elution of the mRNA

was performed with a gradient of 38 % - 70 % of Buffer B. mRNA quality control was performed by spectrophotometry on a 2100 Bioanalyzer (Agilent technologies). Absence of double-stranded RNA (dsRNA) was confirmed using the dsRNA-specific mAb J2 (Scicons) as described elsewhere (*6*).

Preparation and injection of mRNA-LPX. Slightly negatively charged, lymphoid APC-targeting mRNA-LPX were prepared under sterile and RNase-free conditions as described previously (*3*). In all experiments a total volume of 200 µl of mRNA-LPX solution was injected per mouse intravenously (i.v.) into the retrobulbar venous plexus or tail vein.

Preparation and injection of HA saRNA-LNP. LNPs were prepared under sterile conditions containing hemagglutinin (HA) RNA. The hind leg of the mice were shaved and 1 µg of the influenza-heamagglutinin-encoding replicon RNA, formulated in LNPs were injected per mouse intramuscular (i.m) into the musculus gastrocnemius.

Immunization of naïve mice. For immunogenicity studies wild-type C57BL/6 mice or Thy1.1$^+$ 2D2 Foxp3-eGFP TCR-transgenic C57BL/6 mice were injected on days 0, 3, 7 and 10 with 20 µg MOG_{35-55} m1Ψ or U mRNA-LPX, 20 µg irrelevant m1Ψ mRNA-LPX or saline as control. On day 13 spleens were isolated for MOG_{35-55}-specific CD4$^+$ T cell analysis by flow cytometry.
To investigate induction of potent CD8 T cell responses mice were additionally treated at days 6 and 13 with 40 µg $OVA_{257-264}$ U mRNA-LPX or saline as control. Antigen-specific CD8$^+$ T cells were determined five days after last immunization.
Induction of protective immune responses was analyzed after additional application of 1 µg HA-encoding saRNA at day 6 under the same treatment regime. Control mice were treated with saline. HA-specific IgG levels and virus neutralizing titers (VNT) were analyzed 28 days after HA saRNA injection.

Antibodies and flow cytometric analysis. Fluorescence-activated cell sorting (FACS) surface and intracellular antibodies (BTLA, CCR6, CCR7, CD11b, CD11c, CD19, CD25, CD3, CD4, CD40, CD44, CD49b, CD5, CD62L, CD69, CD8, CD80, CD86, CD90.1, CTLA-4, Foxp3, ICOS, IFNγ, IL-17A, LAG-3, KLRG1, MHC-II, PD-1, PD-L1, RORγt, T-bet, TIGIT and TIM-3) were purchased from eBioscience, Bioledgend or BD Pharmingen and used in accordance with the manufacturer's protocol. Single cell suspensions were stained for 30 min at 4 °C for extracellular markers. Chemokine receptors were stained at 37 °C for 30 min and subsequently

fixed with stabilizing fixative (BD Biosciences) for 30 min at 4 °C. For intracellular cytokine staining (ICS) of IFNγ and IL-17A, cells were stimulated in culture medium containing either MOG_{35-55} or $PLP_{139-151}$ peptide (conc. 15 µg/ml), Monensin (GolgiStop, BD Biosciences) and Brefeldin A (Sigma) at 37 °C, for 6 h. After performing live-dead staining (fixable viability dye APCeFluor® 780, eBioscience) and staining of cell-surface markers, cells were fixed and permeabilized using Cytofix/Cytoperm and Perm/Wash buffer from BD Biosciences according to the manufacturer's protocol. Cells were incubated for 30 min at 4 °C with intracellular antibodies and washed twice with Perm/Wash before FACS analysis. Samples were acquired on a BD FACSCanto II, BD FACSCelesta or BD LSR Fortessa and analyzed using FlowJo 7.6.5 or FlowJo 10.4 software (Tree Star). For intracellular staining of Foxp3, CTLA-4, RORγt and T-bet the Foxp3 transcription factor staining buffer set (Thermo Fisher Scientific) was used for fixation and permeabilization. Extracellular staining was performed according to the manufacturer's recommendation. MOG_{35-55}-specific $CD4^+$ T cells were detected by tetramer staining using an APC-conjugated pMHC class II tetramer (National Institutes of Health Tetramer Core Facility). Single cell suspensions of mouse splenocytes were incubated with MOG_{35-55} APC-conjugated tetramer for 1 h at room temperature in culture medium. Cells were washed and anti-APC staining and subsequent anti-APC MACS were performed. Cells were incubated with extracellular or intracellular antibodies as described above. For additional cell sorting of MOG_{35-55}-specific $CD4^+$ T cells, cells were stained with live-dead dye (APCeFluor® 780, eBioscience) and MOG_{35-55}-specific $CD4^+$ T cells were then sorted on a FACSAria cell sorter (BD Biosciences) according to their surface marker expression. Absolute cell counts (total cell infiltrates, $CD3^+$, $CD8^+$, $CD4^+$, $Thy1.1^+$ 2D2 $CD4^+$ T cells) in single cell suspensions of spleen, brain and spinal cord were determined with Trucount™ Tubes (BD Biosciences) by flow cytometry.

Identification of OVA-specific $CD8^+$ T cells was performed with H-$2K^b$/$OVA_{257-264}$ Tetramer (Beckman-Coulter) as previously described (*42*).

***In vivo* bioluminescence imaging.** Albino C57BL/6 mice immunized with 20 µg mRNA-LPX encoding firefly Luciferase (LUC) were injected 6, 24, 48 and 72 h later with an aqueous solution of D-luciferin (250 µl, 1.6 mg; BD Biosciences) intraperitoneally. After 5 min, *in vivo* bioluminescence intensities from the spleen were determined from manually defined regions of interest (ROI) and quantified as total flux (photons/sec) using IVIS Living Image 4.0 Software on the Xenogen IVIS Spectrum *in vivo* imaging system (Caliper Life Sciences). The LUC signal

intensity of emitted photons of live animals was depicted as a color-scaled image, where blue is the least intense and red the most intense bioluminescence signal.

***In vivo* proliferation and adoptive cell transfer.** Splenic $CD4^+$ 2D2 transgenic T cells from naïve 2D2 TCR-transgenic $Th1.1^+$ C57BL/6 mice were isolated using L3T4 microbeads and MACS LS columns (Miltenyi Biotec). For *in vivo* proliferation assays cells were additionally labelled with CTV (CellTrace Violet cell proliferation kit, Thermo Fisher Scientific) and $7x10^6$ cells were injected i.v. into the retrobulbar venous plexus of naïve C57BL/6 ($Thy1.2^+$) mice. On the day after, C57BL/6 mice were immunized with 20 µg MOG_{35-55} m1Ψ or U mRNA-LPX. Control mice received either 20 µg irrelevant m1Ψ mRNA-LPX or saline. Four days after CD4 T cell transfer, proliferation of cells was analyzed by flow cytometry. In other experiments, $7\text{-}10x10^6$ CD4-enriched 2D2 transgenic T cells were injected i.v. into the retrobulbar venous plexus of naïve C57BL/6 ($Thy1.2^+$) mice. On the day after, EAE was actively induced in C57BL/6 mice.

***In vivo* cytokine secretion.** C57BL/6 mice were injected i.v. with 20 µg of the respective mRNA-LPX or saline and sera were collected 6 h after immunization. Secretion of IFNα was determined by IFNα ELISA (PBL) and various other cytokines with a Luminex multiplex cytokine assay (17-plex mouse ELISA assay kit, Thermo Fisher Scientific).

***In vivo* anti-MOG_{35-55} autoantibody detection.** Serum levels of anti-MOG_{35-55} IgG autoantibodies were determined by ELISA (anti-MOG_{35-55} IgG ELISA Kit, Creative Diagnostics) according to manufacturer's instructions. C57BL/6 mice were induced for EAE with MOG_{35-55} peptide and immunized on days 7 and 10 after disease induction with 20 µg MOG_{35-55} m1Ψ mRNA-LPX, 20 µg irrelevant m1Ψ mRNA-LPX or saline. Serum was taken on days -3, 7, 14, 21 and 28. In another experiment F1 C57BL/6 x SJL mice were induced for EAE with $PLP_{139-151}$ peptide and immunized two times per week starting on day 7 after EAE disease induction with 20 µg and 40 µg MOG_{35-55} m1Ψ mRNA-LPX or 20 µg irrelevant m1Ψ mRNA-LPX. Serum was taken on day 50.

***In vivo* anti-HA antibody detection.** Serum levels of mice immunized with HA saRNA were detected via ELISA. For ELISA, recombinant Cf4/H1N1-HA protein (Life Sciences, Id-stein, Germany) was biotinylated utilizing the EZ-Link Sulfor-NHS-LC-biotinylation kit according to supplier's protocol (Thermo Fisher Scientific, Germany). 96-well streptavidin plates (VWR,

Darmstadt, Germany) were coated with the biotinylated HA protein at 4 °C over-night. Upon washing and blocking, serum samples were screened for HA-specific antibodies by incubation on plates for 1 h at 37 °C before 3, 3',5, 5'-tetramethylbenzidine (TMB) one substrate (BIOTREND, Cologne, Germany) was applied. Colorimetric detection was monitored and optical density read at 450 nm calculated to a wavelength reference of 620 nm (D450–620nm).

Measurement of virus neutraliztion test (VNT). C57BL/6 mice were immunized with HA saRNA once at day 6 under MOG_{35-55} or irrelevant m1Ψ mRNA-LPX application regime (days 0, 3, 7 and 10). Injection was performed i.m. For antibody analysis, blood samples were taken under isoflurane anesthesia via the retroorbital venous plexus on day 28 after the first immunization. Virus neutralization test (VNT) to determine VN antibodies in the serum was performed based on the WHO's Manual for the Laboratory Diagnosis and Virological Surveillance of Influenza (WHO Global Influenza Surveillance Network) and as described before (*43*). A serial dilution of serum samples starting with 1:10 was incubated for 2 h with 100 $TCID_{50}$ of infectious influenza virus. The final serum dilution of this assay was 1:1,280 and thereby also the upper detection limit. The serum-virus mix was then applied to confluent monolayer of Madin-Darby canine kidney (MDCK) cells in 96-well plates and incubated for another 3 days. 50 µl of supernatant was thereafter incubated with 50 µl of 0.5% chicken red blood cells (Lohmann Tierzucht, Cuxhaven, Germany), and red blood cell agglutination was evaluated. The VNT titer was recorded as the inverse of the lowest dilution that inhibited agglutination (VNT/50 µl).

***In vivo* cytotoxicity assay.** C57BL/6 mice were immunized under MOG_{35-55} or irrelevant m1Ψ mRNA-LPX application regime (days 0, 3, 7 and 10) two times i.v. with 40 µg SIINFEKL U mRNA-LPX or saline as control (days 6 and 13). Five days after the last immunization, naïve splenocytes were labeled with 0.5 µM (low) or 5 µM (high) CTV (CellTrace Violet cell proliferation kit, Thermo Fisher Scientific). Of these target cells, $1.5x10^6$ cells were adoptively transferred into immunized and control recipients at a ratio of 1:1 (CTV_{low}:CTV_{high}) after loading CTV_{high} cells with SIINFEKL peptide and CTV_{low} cells with irrelevant $HA_{518-526}$ peptide (6 µg/ml), respectively, for 2 h at 37 °C. Recipient splenocytes were recovered and analyzed by flow cytometry 18 h after transfer and antigen-specific lysis was determined as followed: specific lysis (%) = (1-(percentage of cells pulsed with SIINFEKL/percentage of cells pulsed with HA)) x 100).

***In vitro* suppression assay.** CTV-labeled (CellTrace Violet cell proliferation kit, Thermo Fisher Scientific) $CD4^+$ 2D2 transgenic T cells ($3x10^4$ cells per well) of naïve 2D2 TCR-transgenic $Th1.1^+$ C57BL/6 mice were co-cultured with splenic $CD4^+$ 2D2-Foxp3-eGFP transgenic cells of repetitively mRNA-LPX immunized mice. Isolation of $CD4^+$ T cells from total splenocytes was performed using L3T4 microbeads and MACS LS columns (Miltenyi Biotec). Different ratios of suppressor and responder T cells (1:1, 2:1, 4:1, 8:1) were used. 2D2-Foxp3-eGFP mice were injected i.v. on days 0, 3, 7 and 10 with 20 µg m1Ψ or U MOG_{35-55} mRNA-LPX, 20 µg irrelevant m1Ψ mRNA-LPX or saline. The proliferation of CTV-labeled responder cells was analyzed by flow cytometry after restimulation of cells for 72 h with MOG_{35-55} peptide-loaded BMDCs (final concentration 15 µg/ml MOG_{35-55} peptide).

IFNγ enzyme-linked immunospot assay (ELISpot). Frequencies of MOG_{35-55}-responding $CD4^+$ T cells were examined by Interferon γ (IFNγ) ELISpot. Mice were treated on days 0, 3, 7 and 10 with 20 µg m1Ψ or U MOG_{35-55} mRNA-LPX, 20 µg irrelevant m1Ψ mRNA-LPX or saline. On day 13 after first treatment, splenic $CD4^+$ T cells were purified by MACS using CD4 (L3T4) microbeads and LS columns (Miltenyi Biotec) and $5x10^5$ $CD4^+$ T cells were cultured with $1x10^5$ MOG_{35-55} peptide-loaded BMDCs (peptide-concentration 15 µg/ml) for 18 h at 37 °C in anti-IFNγ (10 µg/ml, clone AN18, Mabtech) coated Multiscreen 96-well plates (Merck Millipore). Cytokine secretion was detected with a biotin-conjugated secondary anti-IFNγ antibody (1 µg/ml, clone R4-6A2, Mabtech). Visualization of secondary antibody was mediated by adding ExtrAvidin-Alkaline phosphatase (Sigma-Aldrich) and BCIP/NBT liquid substrate (Sigma-Aldrich). Quantification of spots was performed on an ELISpot Reader (S6 Macro Analyzer; CTL) and analyzed using ImmunoSpot software. All samples were tested in triplicates.

For analysis of T cell responses against SIINFEKL, $5x10^5$ total splenocytes were restimulated with 2 µg/ml respective peptide. All other steps were performed to the above described protocol.

Synthetic peptides. MOG_{35-55} (MEV GWY RSP FSR VVH LYR NGK), $PLP_{139-151}$ (HSL GKW LGH PDK F), $PLP_{178-191}$ (NTW TTC QSI AFP SK), MBP_{84-104} (VHF FKN IVT PRT PPP SQG KGR), $MOBP_{15-36}$ (QKF SHE FSI HCC PPF TFL NSK R), $OVA_{257-264}$ (SII NFE KL), $HA_{518-526}$ (IYS TVA SSL) peptides were obtained from JPT Peptide Technologies GmbH.

EAE models. Acute experimental autoimmune encephalomyelitis (EAE) was induced in female C57BL/6 mice (8-10 weeks) with 50 µg of MOG_{35-55} peptide emulsified in CFA (Difco

Laboratories) supplemented with 10 mg/ml of heat-inactivated Mycobacterium tuberculosis H37RA (Difco Laboratories) subcutaneously at the base of the tail. The mice received 200 ng Pertussis toxin (PTX) (List Biological Laboratories, INC., Campbell, CA) intraperitoneally on the day of immunization and 2 days later. Starting on day 10 after immunization mice were daily weighed and scored for clinical symptoms according to the following criteria: 0, no disease; 1, decreased tail tone; 2, impaired righting reflex; 3, partial hind limb paralysis; 4, complete hind limb paralysis; 5, hind limb paralysis with partial fore limb paralysis; and 6, moribund or dead. Relapsing-remitting EAE was induced in female SJL/JRj mice (8-10 weeks) or female F1 hybrid mice from C57BL/6 and SJL/JRj background (8-10 weeks) with 200 µg of $PLP_{139-151}$ peptide emulsified in CFA supplemented with 10 mg/ml of heat-inactivated Mycobacterium tuberculosis H37RA s.c. at the base of the tail. The mice received 200 ng PTX intraperitoneally on the day of immunization and 2 days later. Starting on day 8 mice were weighed and scored for clinical symptoms daily. In addition to the criteria above, the following ones were used: 2, at least one hind leg falls through a wire rack; 3, strong head tilt. Complex EAE was induced in female F1 hybrid mice from C57BL/6 and SJL/JRj (8-10 weeks) with a peptide mixture consisting of 50 µg of each MOG_{35-55}, $PLP_{139-151}$, $PLP_{178-191}$ MBP_{84-104}, $MOBP_{15-36}$. The peptide mixture was emulsified in CFA supplemented with 10 mg/ml of heat-inactivated Mycobacterium tuberculosis H37RA and injected s.c. at the base of the tail. The mice received 200 ng PTX intraperitoneally on the day of immunization and 2 days later. Mice were weighed and scored for clinical symptoms daily starting on day 8 after immunization according to scoring criteria described above.

mRNA-LPX treatment of EAE mice. To determine protective immunity in C57BL/6 EAE mice, mice were treated with 20 µg MOG_{35-55} m1Ψ, 20 µg irrelevant m1Ψ mRNA-LPX or saline unless stated otherwise on days 7 and 10 or at an EAE score of 1-2 after disease induction. SJL/JRj mice with manifest relapsing-remitting EAE were treated with 20 µg $PLP_{139-151}$ m1Ψ mRNA-LPX on days 7 and 10 after EAE induction, twice per week starting on days 7 and 10 after disease induction. In a second experiment, SJL/JRj mice were treated starting on days 14 and 17 with the same treatment groups. In experiments comparing single-epitope m1Ψ mRNA-LPX treatment with multi-epitope treatment, complex EAE mice were treated with 40 µg multi-epitope encoding m1Ψ mRNA (10 µg of each epitope-encoding m1Ψ mRNA (MOG_{35-55}, $PLP_{139-151}$, $PLP_{178-191}$, MBP_{84-104}) was used), 10 µg MOG_{35-55} m1Ψ mRNA or 10 µg irrelevant control m1Ψ mRNA. mRNA-LPX was injected twice per week starting on days 7 and 10 after EAE induction. For investigating bystander suppression in EAE, F1 hybrid mice from C57BL/6

and SJL/JRj were treated twice weekly with 20 or 40 µg MOG_{35-55} m1Ψ mRNA-LPX, 20 µg $PLP_{139-151}$ m1Ψ mRNA-LPX, 20 µg irrelevant mRNA-LPX or saline as control starting on days 7 and 10 after EAE disease induction. In a second experiment, EAE mice were treated with 40 µg of m1Ψ mRNA-LPX encoding several different epitopes.

Antibody treatment. C57BL/6 EAE mice were treated with PD-1 (500 µg first two treatments, 250 µg following treatments, clone RMP1-14, BioXcell), or CTLA-4 (500 µg first two treatments, 250 µg following treatments, clone 9H10, BioXcell) blocking antibody or isotype-matched control antibodies (rat IgG2a and syrian hamster IgG, BioXcell) on days 7, 10, 14 and 17 after EAE induction. Antibodies were diluted in PBS and applied intraperitoneally.

Tissue preparation for single cell suspensions. All cell-based analyses were performed on single cell suspensions of blood, spleen, brain and spinal cord. In brief, peripheral blood was collected from the vena facialis. Spleens were mashed through a 70-µm cell strainer (BD-Falcon) using the plunger of a 5-ml syringe (BD Biosciences) while rinsing with PBS. Erythrocytes were removed by hypotonic lysis. For analysis of CNS-infiltrated lymphocytes (from brain and spinal cord), mice were anesthetized with ketamine-rompun and perfused with 0.9 % NaCl through the heart left ventricle. The brain and spinal cord were removed manually, cut into small pieces and digested in PBS++ (Gibco) containing collagenase D (1 mg/ml; Roche) and DNase I (0.1 mg/ml; Roche) for 20 min at 37 °C. The digested tissue was homogenized manually by sucking up the tissue pieces into a syringe and pressing out against the wall of a falcon tube. The single cell suspension was resuspended in 70 % Percoll (GE Healthcare) and layered under a 30:37 percoll gradient. The final percoll gradient was centrifuged at 300 g for 40 min at room temperature. The lymphocyte cell layer was collected at the interphase between 70 % and 37 % percoll and washed with 2 % FCS/PBS before further analyses.

Isolation and *in vitro* stimulation of splenocytes. Splenic $CD4^+$ T cells of C57BL/6 mice treated on days 0, 3, 7 and 10 with MOG_{35-55} m1Ψ or U mRNA-LPX, irrelevant m1Ψ mRNA-LPX or saline were isolated 3 days after the last immunization using L3T4 microbeads and MACS LS columns (Miltenyi Biotec). 3x 10^4 $CD4^+$ T cells were stimulated for 48 h with MOG_{35-55} peptide-loaded (0, 5, 10, 20 and 100 µg/ml) BMDCs (3x 10^4 cells) and the supernatants were analyzed for cytokine content with a Luminex multiplex cytokine assay (17-plex mouse ELISA assay kit, Thermo Fisher Scientific).

Immunohistochemistry. Spinal cords were harvested, fixed with 4 % histofix overnight at 4 °C and embedded in paraffin blocks. 3 µm sections of tissue were stained with LFB. Briefly, after deparaffinization and rehydration, sections were incubated in LFB solution (1:100 w/v) overnight at 60 °C and counterstained with eosin. Additional sections were stained by immunohistochemistry using a rabbit anti-mouse CD4 antibody (1:8000, Sino Biologicals, 50134-R001) and the staining is detected using a streptavidin-HRP system (Vector Labs). Light microscope images were taken using the Zeiss AxioImager M2 and analyzed using ZEN blue software.

Preparation and sequencing of single cell 3´-libraries. FACS sorted tetramer$^+$ CD4$^+$ living cells were filtered with a 40 µm Flowmi™ Cell Strainer (Bel-Art), centrifuged and resuspended with 1X PBS with 0.04 % BSA. Final single-cell suspensions were processed according to 10X Genomics Chromium Single Cell 3´ Reagent Guidelines (v2 chemistry: CG00052 Rev D). Shortly, cells were partitioned into nanoliter-scale gel bead-in-emulsions (GEMs) using 10X Chromium Controller. During reverse transcription reaction with a C1000 Touch Thermal Cycler (Bio-Rad), polyadenylated mRNA from partitioned and lysed cells were incubated with primers containing (i) an Illumina R1 sequence, (ii) a 16 bp 10X barcode, (iii) a 10 bp Unique Molecular Identifier (UMI) and (iv) a poly-dT primer sequence resulting in barcoded, full-length cDNA. cDNA was purified using Silane magnetic beads (Thermo Fisher) and amplified by PCR. During library construction via fragmentation, end repair, A-tailing, adaptor ligation, post-ligation cleanup with SPRIselect (Beckmann Coulter), index PCR and cleanup, the following sequences were added: P5 and P7 (Illumina sequence), a sample index (i7), and R2 (read 2 primer sequence). Quantification of cDNA and final libraries were performed using Qubit dsDNA HS Assay Kit (Life Technologies) and High-sensitivity DNA Chips (Agilent). Final libraries were diluted to 250 pM, pooled and loaded on an Illumina HiSeq4000 platform with 2x 150 paired-end kits for sequencing resulting in more than 150,000 reads per cell with the following read lengths: 26 cycles (Read 1), 8 cycles (i7 Index) and 98 cycles (Read 2).

Single-cell RNA sequencing raw data processing. The 10X Genomics Cellranger single-cell pipeline (v2.1.1) was used to perform sample demultiplexing, barcode processing and single-cell 3´ gene counting, as previously described (*44*). Briefly, sample demultiplexing was performed based on the 8 bp sample index read to generate FASTQs for the Read1 and Read2 paired-end reads, as well as the 16 bp 10X barcode by using the Cellranger mkfastq pipeline. Afterwards generated FASTQs were aligned to the mouse mm10 reference genome (v1.2.0) with Cellranger

count pipeline. To generate gene-barcode matrices, aligned reads were filtered for valid UMIs (max. 1 mismatch allowed) with sequencing quality score > 10 (90 % base accuracy), barcodes with UMI counts that fell within the 99th percentile of the range and PCR duplicates were removed. Principal component analysis (PCA) is followed to consider genes with at least one UMI count in at least one cell, whereas the top 1000 most variable genes are identified based on mean and dispersion. Output data of technical replicates for each group were aggregated via "cell ranger aggr" function and were produced a single gene-barcode matrix containing all the data.

Comparative clustering analysis with Seurat's alignment strategy. For clustering analysis, Seurat (v2.3.1) R toolkit (with R version 3.5.0.) (*45*) was used as described in the tutorials (https://satijalab.org/seurat/). Low quality cells with less than 200 genes, more than three median absolute deviation (MADs) above the median mitochondrial genes and more than three MADs above the median gene counts were excluded from the further analysis. Digital gene expression measurements were log-normalized and log-transformed afterwards. The number of detected molecules per cell, the percentage mitochondrial gene content as well as cell cycle effects were regressed out as source of cellular variation for improved downstream dimensional reduction. Cell cycle effects were mitigated using a cell cycle scoring strategy based on Tirosh et al. (*46*) as described by Seurat. Each sample was processed separately until this point, then both samples were combined.

A conserved gene correlation structure was identified by a canonical correlation analysis (CCA) in order to perform an integrated and comparative analysis between two datasets. For cell cluster identification an algorithm was used based on shared nearest neighbor (SNN) modularity optimization, which took the top 20 correlation components (CCs) and a community resolution parameter of 1.4 (*47*). For the visualization, a two-dimensional non-linear embedding of the cells was generated on the first 20 CC dimensions using uniform manifold approximation and projection (UMAP), a Seurat-supported Python package (*48*, *49*). Cells across one condition were grouped together based on shared gene expression patterns. Via differential expression method, positive and negative markers of a single cluster compared to others clusters or to all other remaining cells were identified applying the "Wilcoxon rank sum test" (default). Assignment of cell type identity to clusters was done by using canonical markers and differentially top expressed genes. Despite cell cycle regression analysis, a small population of proliferating cells (*Tyms*, *Birc5*) was detected as separate subpopulation. Moreover, although stringent cut-offs for mitochondrial gene and total gene content were used, a low-quality cell

cluster mainly defined by a low cytoplasmic transcript fraction (to a large extent ribosome-associated genes) and high mitochondrial and nuclear genes (e.g. *Mt-Atp6* and *Malat1*) clustered together. Additionally, a small contamination of a DC population (less than 0.5 %) in both groups, expressing specifically for example *H2-Eb1, H2-Aa, Spi1 and Fcer1g* was found. Those three subpopulations were excluded for further analysis. Furthermore, two clusters sharing typical memory feature without further functionally relevant differences were merged to one cluster as well as two clusters sharing typical central T_{reg} cell features.

Gene set enrichment analysis. Enrichment of selected marker genes (table S2) for respective T cell subsets was assessed via a non-parametric and unsupervised gsva function from the R-package Gene Set Variation Analysis (GSVA, v1.26.0) software using the ssgsea method (*50*).

Single cell trajectory analysis. The R package Monocle 2 (v 2.8.0) (*51*) was used to construct differentiation trajectories in an unsupervised procedure based on genes that differ between clusters identified by Seurat. Monocle 2 is using the strategy of ordering single cells in pseudotime by learning an explicit principal tree from the single cell genomics data with advanced machine learning techniques (Reversed Graph Embedding). Each cell is projected on its nearest location on the principal tree in different states corresponding to a biological process such as cell differentiation. Monocle 2 further assigns branch points, which describe the turnoff in a cellular process with different outcomes (*52*). The cluster information identified by Seurat was used as input for unsupervised pseudotime ordering. Using Monocle 2‘s import function allowed the conversion of Seurat object into the Monocle pipeline, where the determined 20 CC dimensions were used. Genes, which were expressed in at least 50 cells of the data set were used to order the cells along a biological process. Furthermore, cells were ordered based on the genes differentially expressed between clusters identified by Seurat with a q-value < 0.0005 resulting in 2090 ordering genes. Dimension reduction was executed by using maximal 2 components and the reduction method “discriminative dimensionality reduction via learning a tree” (DDRTree). The root of the trajectories was defined manually.

Statistical analysis. Statistical significance was evaluated using GraphPad Prism 7 software (Graphpad Software, Inc.) employing Student’s t-test when two groups were compared or one-way ANOVA corrected with Tukey’s-comparison test factor comparing more than two groups. EAE development was compared by calculating the area under the disease development curve (AUC) for single mice of each treatment group and subsequently compared by one-way

ANOVA. Values of $p \leq 0.05$ were considered to be statistically significant; $*p \leq 0.05$, $**p \leq 0.01$, $***p \leq 0.001$, $****p \leq 0.0001$. The employed tests are referred to in the respective figure legends. Grubb's test was used for identification of outliers (alpha = 0.05).

SUPPLEMENTARY FIGURES & TABLES

Fig. S1. Comparison of m1Ψ vs. U mRNA treatment in naïve mice. (**A**) Activation markers on splenic $CD11c^+$ APCs 24 h after i.v. injection of LPX-formulated mRNAs and saline (control) in C57BL/6 mice (n = 5). (**B**) Cytokine serum levels in C57BL/6 mice (n = 3) 6 h after i.v. injection of LPX-formulated mRNAs and saline (control). Data were compared using one-way ANOVA and post hoc Tukey's test. Error bars indicate mean ± SD.

Fig. S2. Phenotype of 2D2 TCR-transgenic $CD4^+$ T cells upon m1Ψ mRNA application. (**A** to **C**) $Thy1.1^+$ 2D2 Foxp3-eGFP TCR transgenic C57BL/6 mice (n = 4) were treated (days 0, 3, 7, 10) with mRNA or saline (control). Three days after last dosing (**A**) frequency of $Foxp3^+$ T_{reg} cells in spleens were analysed. (**B**) Proliferation of naïve MOG_{35-55}-specific, CTV-labelled $CD4^+$ T cells after 72 h co-culture with MOG_{35-55} peptide-loaded BMDCs and $CD4^+$ T cells of treated mice from (**A**). Percent indicates frequency of divided T_{eff} cells (n = 4). (**C**) Expression of coinhibitory molecules on 2D2 $CD4^+$ T cells three days after last dosing. Data were compared using one-way ANOVA and post hoc Tukey's test. Error bars indicate mean ± SD.

Fig. S3. Cytokine secretion profile of MOG_{35-55}-specific $CD4^+$ T cells. Cytokine secretion of splenic $CD4^+$ T cells 48 h after restimulation with BMDCs loaded with increasing amounts of MOG_{35-55} peptide. $CD4^+$ T cells were derived from mice dosed repeatedly (days 0, 3, 7, 10) with mRNA or saline (control) (n = 4). Data were compared using one-way ANOVA and post hoc Tukey's test. Error bars indicate mean ± SD.

Fig. S4. Treatment with antigen-encoding m1Ψ mRNA during disease progression results in efficient treatment of EAE mice. (**A**) Maximal disease score outcome of each individual MOG_{35-55}-induced EAE mouse (n = 6-9 C57BL/6 mice per group) after starting treatment with m1Ψ mRNA or saline (control) at score 1-2. (**B**-**E**) Characterization of MOG_{35-55}-specific $CD4^+$ T cells by flow cytometry. $Thy1.1^+$ 2D2 $CD4^+$ T cells were transferred into $Thy1.2^+$ recipient C57BL/6 mice one day prior to EAE induction. Mice were treated with m1Ψ mRNA or saline (control) at score 1-2 and cells were analyzed on day 19. (**B**) Total cell number of lymphocytes infiltrated in spinal cord (n = 3-4). (**C**) Frequency of $CD4^+$ IFNγ- and IL-17A-secreting cells in brain and spinal cord after restimulation *ex vivo* in the presence of MOG_{35-55} peptide for 6 h (n = 3-4). (**D**) Frequency and total cell number of MOG_{35-55}-specific $CD4^+$ T cells in the spleen. (**E**) Phenotypic analysis of splenic MOG_{35-55}-specific $CD4^+$ T cells from (**D**). Data were compared using one-way ANOVA and post hoc Tukey's test. Error bars indicate mean ± SD.

Fig. S5. Altered MOG_{35-55}-specific $CD4^+$ T cell frequencies and total cell count in spleen and CNS. Naïve $Thy1.1^+$ 2D2 $CD4^+$ donor T cells were adoptively transferred into $Thy1.2^+$ C57BL/6 mice on day -1. EAE was induced with MOG_{35-55} peptide and mice were treated with m1Ψ mRNA or saline (control) on days 7 and 10 after EAE induction. Infiltration of $CD3^+$, $CD8^+$, $CD4^+$ and $Thy1.1^+$ $CD4^+$ MOG_{35-55}-specific T cells was analysed on day 16 and the total number of infiltrated cells was determined via flow cytometry using Trucount™ tubes. Data are depicted as mean ± SD from n = 3-4 mice/group. Statistical analysis of infiltrated cells was assessed via one-way ANOVA and Tukey's multiple comparison test.

Fig. S6. Expression of specific adhesion molecules and chemokine receptors on MOG_{35-55}-specific $CD4^+$ T cells upon mRNA treatment in EAE mice. MOG_{35-55}-peptide induced EAE mice (C57BL/6) were treated with m1Ψ mRNA or saline (control) on days 7 and 10 after EAE induction. Flow cytometry analysis of splenic $tetramer^+$ $CD4^+$ T cells (n = 5-6) was performed on day 16 after EAE induction. Statistical analysis was assessed via one-way ANOVA and Tukey's multiple comparison test. Error bars indicate mean ± SD.

Fig. S7. Induction and maintenance of antigen-encoding m1Ψ mRNA-induced tolerance is independent of the EAE disease model and mediated by bystander immunosuppression. (**A** and **B**) Dynamics of EAE in $PLP_{139-151}$-induced EAE mice (n = 8-10 SJL mice) (**A**) upon treatment with m1Ψ mRNA ($PLP_{139-151}$ m1Ψ mRNA administered either on days 7 and 10 only or continued twice per week) and (**B**) upon treatment with m1Ψ mRNA ($PLP_{139-151}$ m1Ψ mRNA on days 14 and 17 only or continued twice per week). (**C**) Dynamics of EAE in $PLP_{139-151}$-induced EAE mice (n = 8-10 F1 C57BL/6 x SJL mice) upon treatment with MOG_{35-55} m1Ψ, $PLP_{139-151}$ m1Ψ, irrelevant m1Ψ mRNA or saline (control) twice per week starting on days 7 and 10 after disease induction. (**D**) EAE model based on autoreactivity concurrently against MOG_{35-55}, $PLP_{139-151}$, $PLP_{178-191}$, MBP_{84-104} and $MOBP_{15-36}$ induced in F1 C57BL/6 x SJL mice (n = 6-8). Dynamics of the disease after treatment with either MOG_{35-55} m1Ψ mRNA alone, with a mixture of m1Ψ mRNA encoding MOG_{35-55}, $PLP_{139-151}$, $PLP_{178-191}$ and MBP_{84-104} autoantigen epitopes or irrelevant m1Ψ mRNA twice per week starting on days 7 and 10 after disease induction. AUC was used to determine statistical significance via one-way ANOVA and Tukey's multiple comparison test of the different EAE disease development curves. Error bars indicate mean ± SEM.

Fig. S8. Anti-MOG_{35-55} IgG antibodies in response to MOG_{35-55} m1Ψ mRNA vaccination. (**A**) EAE was induced by immunization with MOG_{35-55}-CFA emulsion (day 0) and PTX (days 0 and 2) and mice were treated with m1Ψ mRNA or saline (control) on days 7 and 10 after EAE induction. Sera were taken on days -3, 7, 14, 21 and 28. Individual values are plotted for each mouse, as well as mean of each group from n = 8 mice/group. Dashed line indicates baseline levels measured on day -3. (**B**) EAE was induced in F1 C57BL/6 x SJL by immunization with $PLP_{139-151}$-CFA emulsion (day 0) and PTX (days 0 and 2) and mice were vaccination with 20 or 40 µg MOG_{35-55} m1Ψ mRNA or irrelevant m1Ψ twice per week starting at day 7 after EAE induction. At day 50 sera were collected. Statistical analysis was assessed via one-way ANOVA and Tukey's multiple comparison test.

Fig. S9. Transcriptome analysis of MOG_{35-55}-specific $CD4^+$ T cells by single-cell RNA sequencing. Heatmap of the top ten expressed genes for each of the eight different T cell subpopulations detected in MOG_{35-55}-specific $CD4^+$ T cells split into treatment groups.

Fig. S10. Canonical marker expression in MOG_{35-55}-specific $CD4^+$ T cell. (**A**) Marker expression for common CD4 T cell markers visualized in UMAP plots and violin plots as quality control for sequencing analysis. Cd8a shows no detectable expression. (**B**) UMAP projection of single cells, colour-coded according to the identified cell-subsets.

Fig. S11. Canonical marker expression of different MOG_{35-55}-specific $CD4^+$ T cell subpopulations. (**A** to **H**) Subset-specific marker expression for identified CD4 T cell subpopulations was visualized and plotted for different clusters in UMAP plots and violin plots in comparison to UMAP projection of single cells with colour-coding of the identified cell-subsets (**I**).

Fig. S12. Heatmap showing gene set enrichment scores for predefined subset-specific gene sets (**A**) and averaged expression for individual genes from respective gene sets (**B**) for identified T cell clusters across conditions.

Fig. S13. Characterization of different MOG_{35-55}-specific $CD4^+$ T cell subpopulations revealed by single-cell RNA sequencing. (**A**) Subset-specific genes for central and effector T_{reg} cells. Genes characteristic for exhausted (**B**) and T_{FH} (**C**) cell clusters.

Fig. S14. Genes found to be differentially expressed in MOG_{35-55}-specific $CD4^+$ T cell subpopulations by single-cell RNA sequencing. (**A**) Genes upregulated upon MOG_{35-55} m1Ψ mRNA treatment in T_H1, T_H17 and T_H1/T_H17 cell subsets (adjusted p-value < 0.05). (**B**) Genome integrity and cell cycle-related genes in pathogenic subsets.

Fig. S15. Pseudotime ordering of MOG_{35-55}-specific $CD4^+$ T cells. (**A** to **D**) Single cell trajectory analysis of MOG_{35-55}-specific $CD4^+$ T cells by Monocle 2. Each dot represents a single cell coloured by pre-identified cell-subsets, whereas its location between different branch points of the trajectory tree (indicated by black lines) reflects the state. (**A**) Overlay of all cell clusters from both treatment groups, in which cells were placed in seven different states. (**B**) Trajectory plot showing each cell upon MOG_{35-55} m1Ψ mRNA treatment in blue and for irrelevant m1Ψ mRNA treatment in grey. (**C** and **D**) Split trajectory plots for treatment with (**C**) MOG_{35-55} m1Ψ and (**D**) irrelevant m1Ψ mRNA. (**E**) Pseudotime trajectory showing cells from both treatment groups. Cells are highlighted by pseudotime ranging from 0 to 12.5. (**F**) Distribution of MOG_{35-55}-specific $CD4^+$ T cell subsets among the different states of (**A**).

Fig. S16. Expression of Ctla4 and PD-1 on MOG_{35-55}-specific $CD4^+$ T_{reg} and T_{eff} cell subsets. (**A**) Flow cytometry analysis of CTLA-4 and PD-1 on splenic MOG_{35-55}-specific $CD4^+$ $tetramer^+$ T cells in MOG_{35-55}-induced EAE mice, treated with m1Ψ mRNA or saline (control) on days 7 and 10 after disease induction and analysed on day 16. (**B**) Subset specific gene expression of *Ctla4* for T_{reg} cell clusters and other subsets detected by scRNA seq.

Table S1. Sequencing statistics. Single-cell RNA sequencing data from technical replicates of each treatment group were aggregated and a single gene-barcode matrix was generated for further analysis.

Table S2. List of individual genes generating the subset-specific gene sets. Gene sets were created from known markers for different T cell subsets.

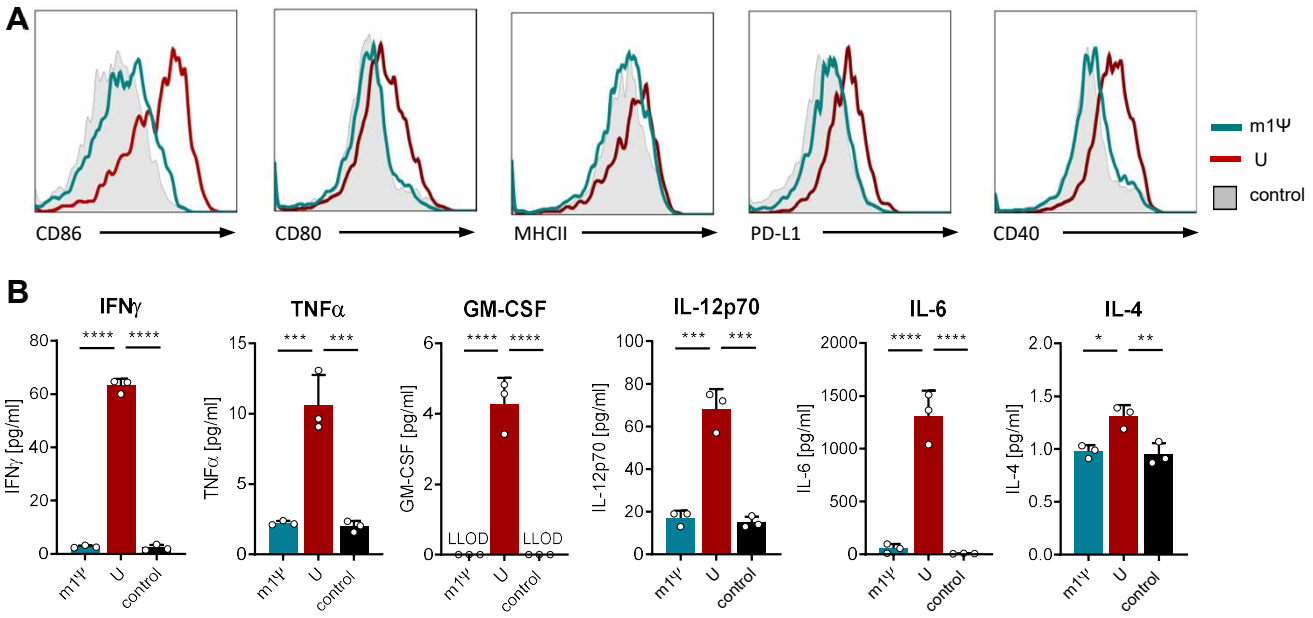

Fig. S1. Comparison of m1Ψ vs. U mRNA treatment in naïve mice.

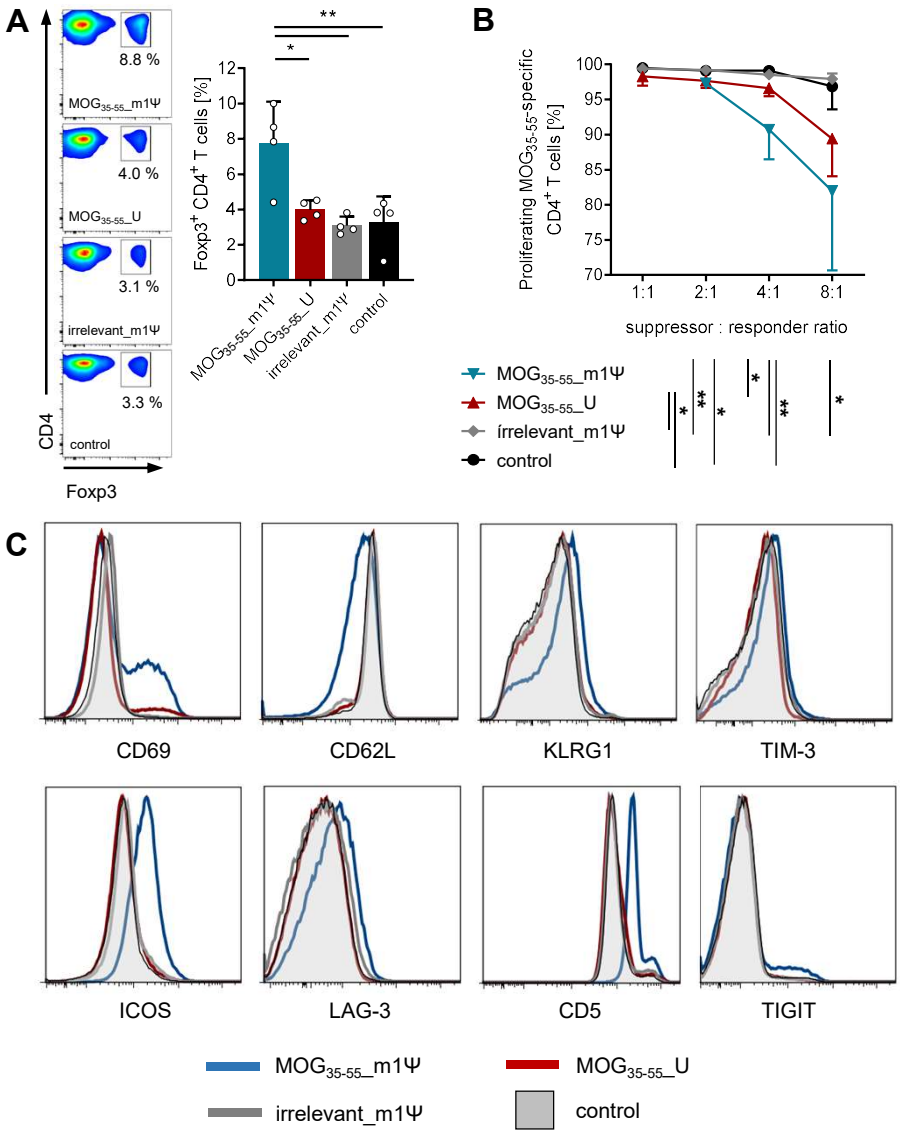

Fig. S2. Phenotype of 2D2 TCR-transgenic CD4+ T cells upon m1Ψ mRNA application.

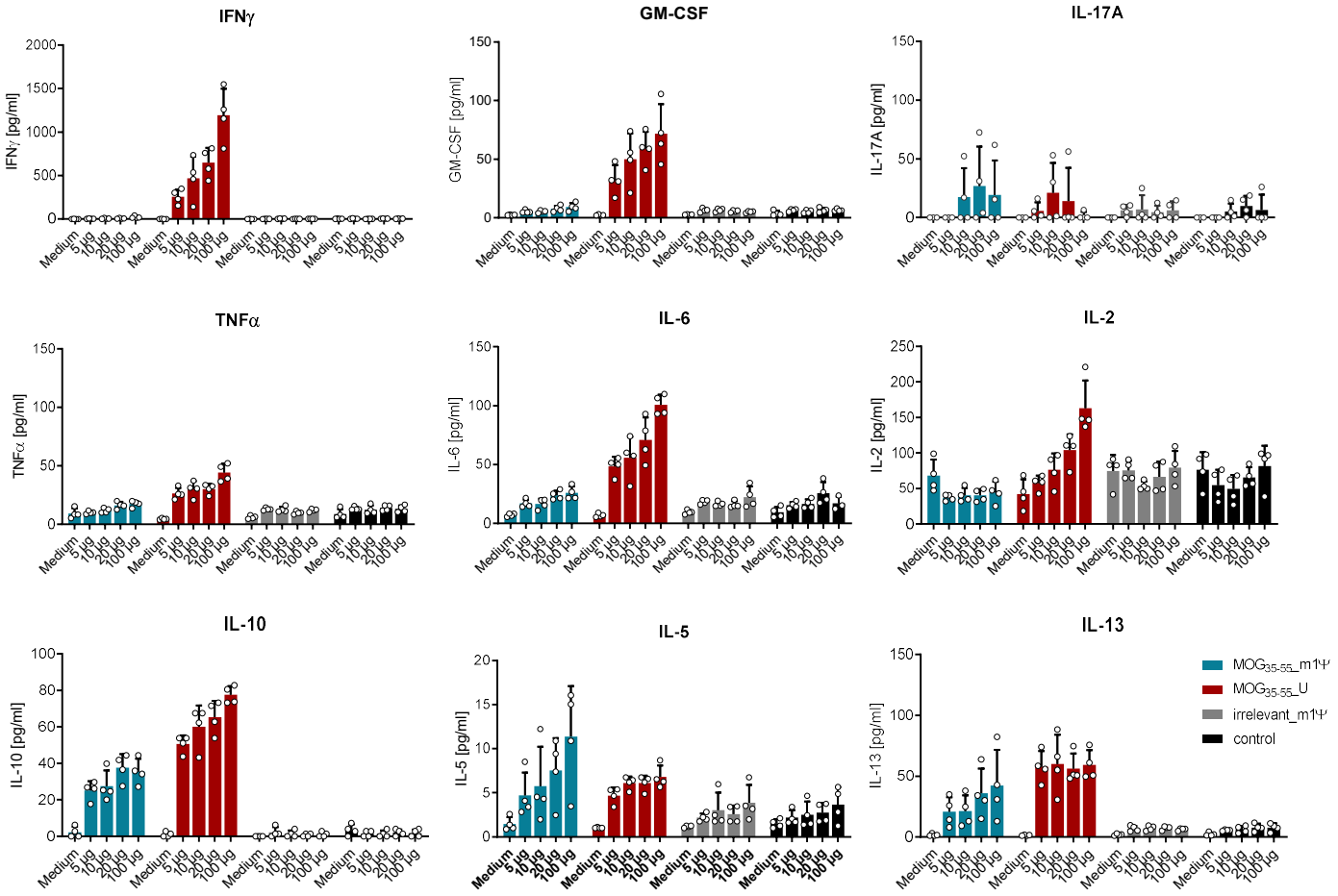

Fig. S3. Cytokine secretion profile of MOG_{35-55}-specific CD4+ T cells

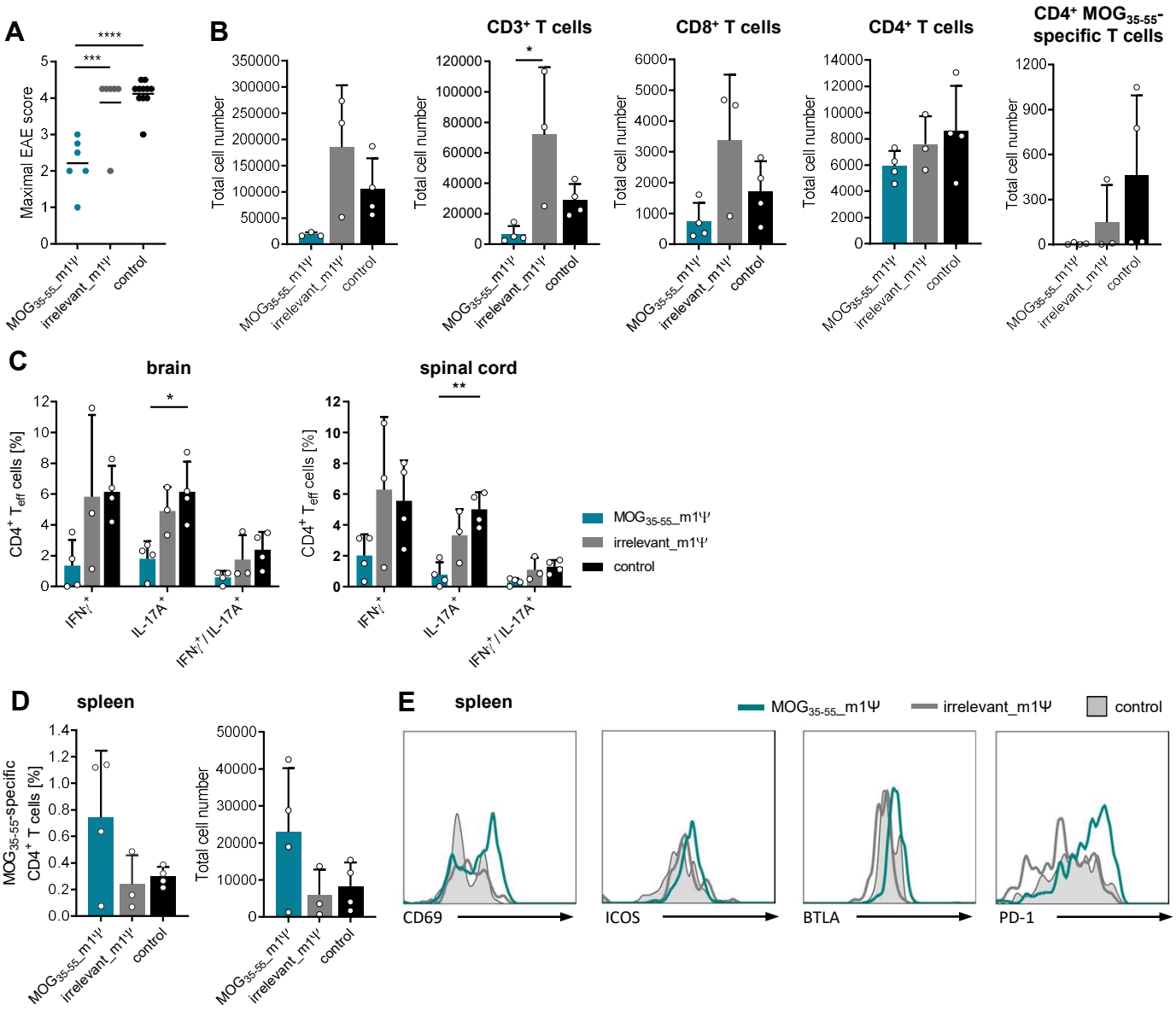

Fig. S4 Treatment with antigen-encoding m1Ψ mRNA during disease progression results in efficient treatment of EAE mice.

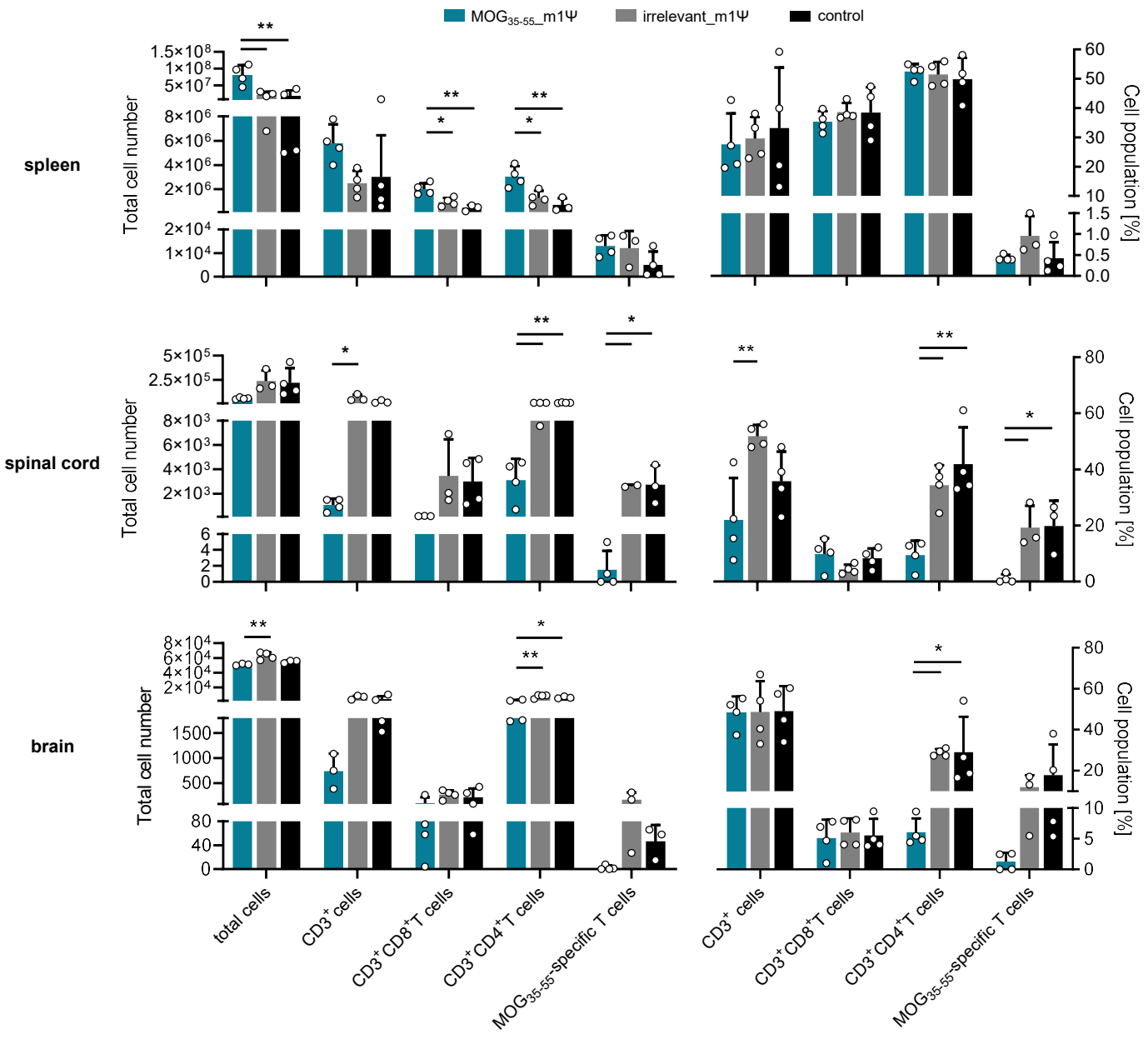

Fig. S5. Altered MOG_{35-55}-specific $CD4^+$ T cell frequencies and total cell count in spleen and CNS.

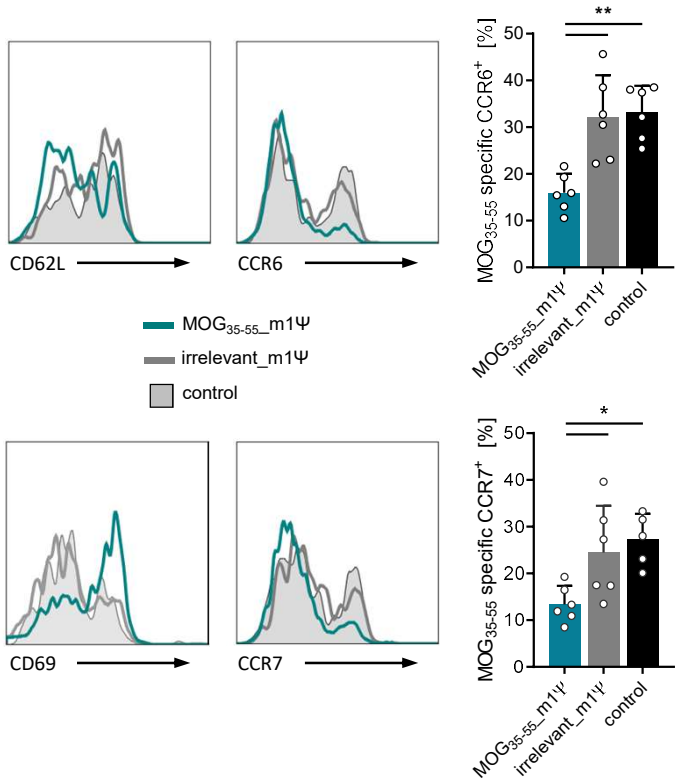

Fig. S6. Expression of specific adhesion molecules and chemokine receptors on MOG_{35-55}-specific $CD4^+$ T cells upon mRNA treatment in EAE mice.

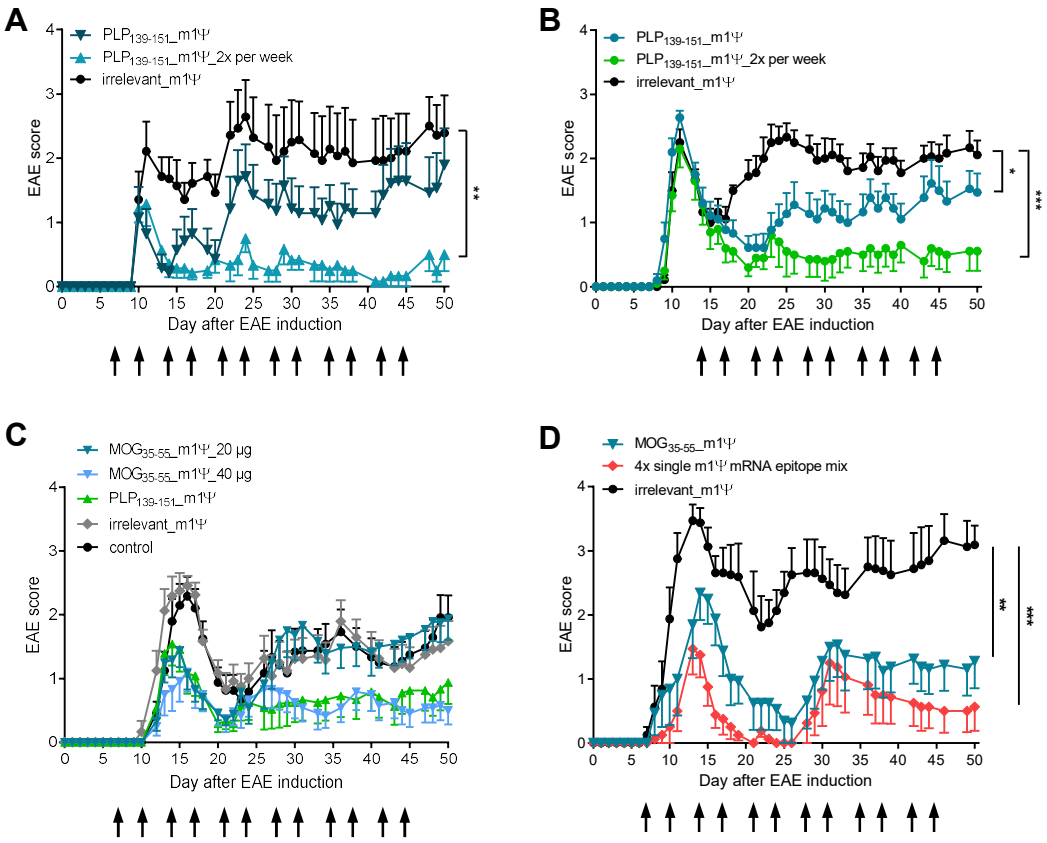

Fig. S7. Induction and maintenance of antigen-encoding m1Ψ mRNA-induced tolerance is independent of the EAE disease model and mediated by bystander immunosuppression.

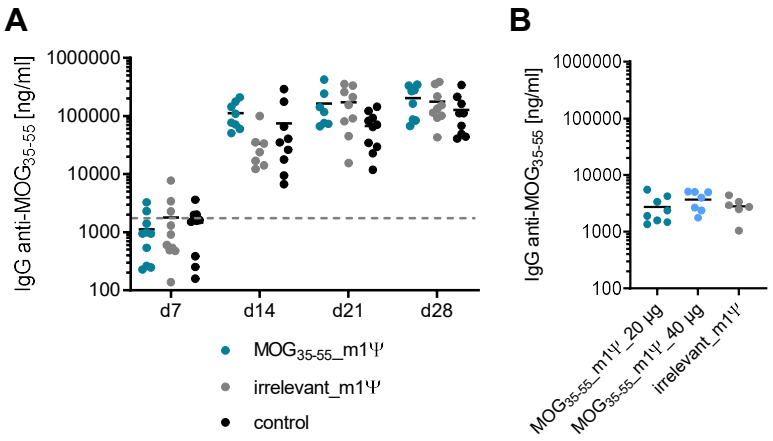

Fig. S8. Anti-MOG_{35-55} IgG antibodies in response to MOG_{35-55} m1Ψ mRNA vaccination.

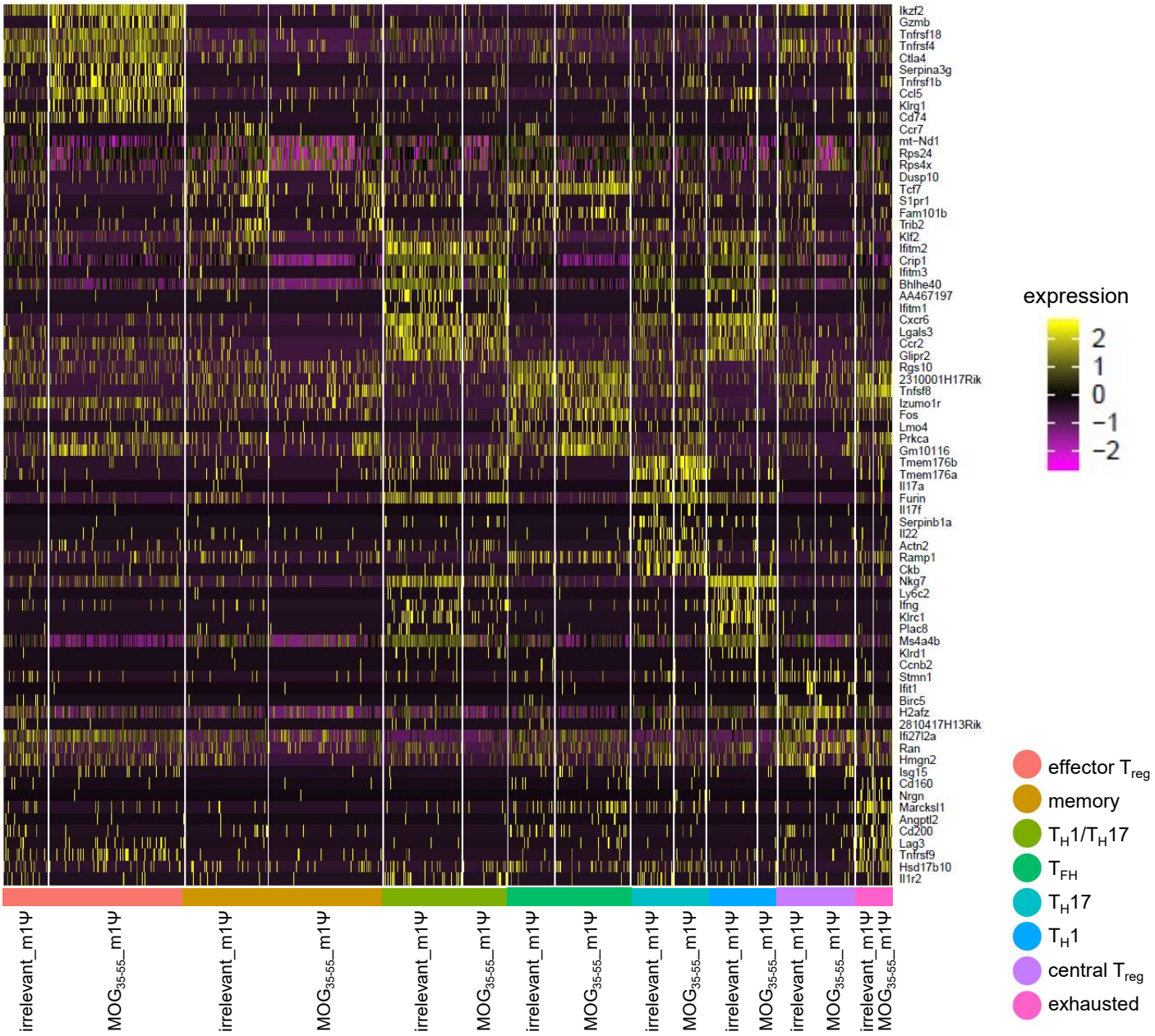

Fig. S9. Transcriptome analysis of MOG_{35-55}-specific $CD4^+$ T cells by single-cell RNA sequencing.

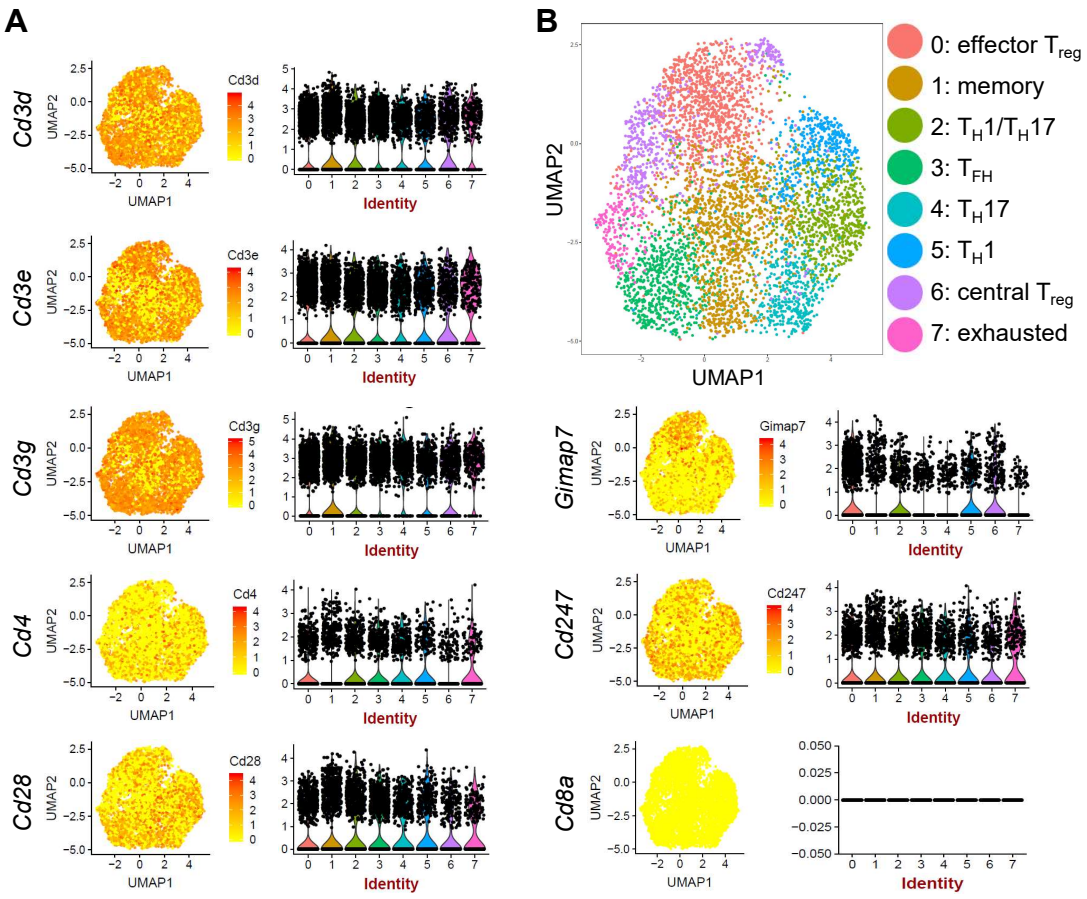

Fig. S10. Canonical marker expression in MOG_{35-55}-specific $CD4^+$ T cell.

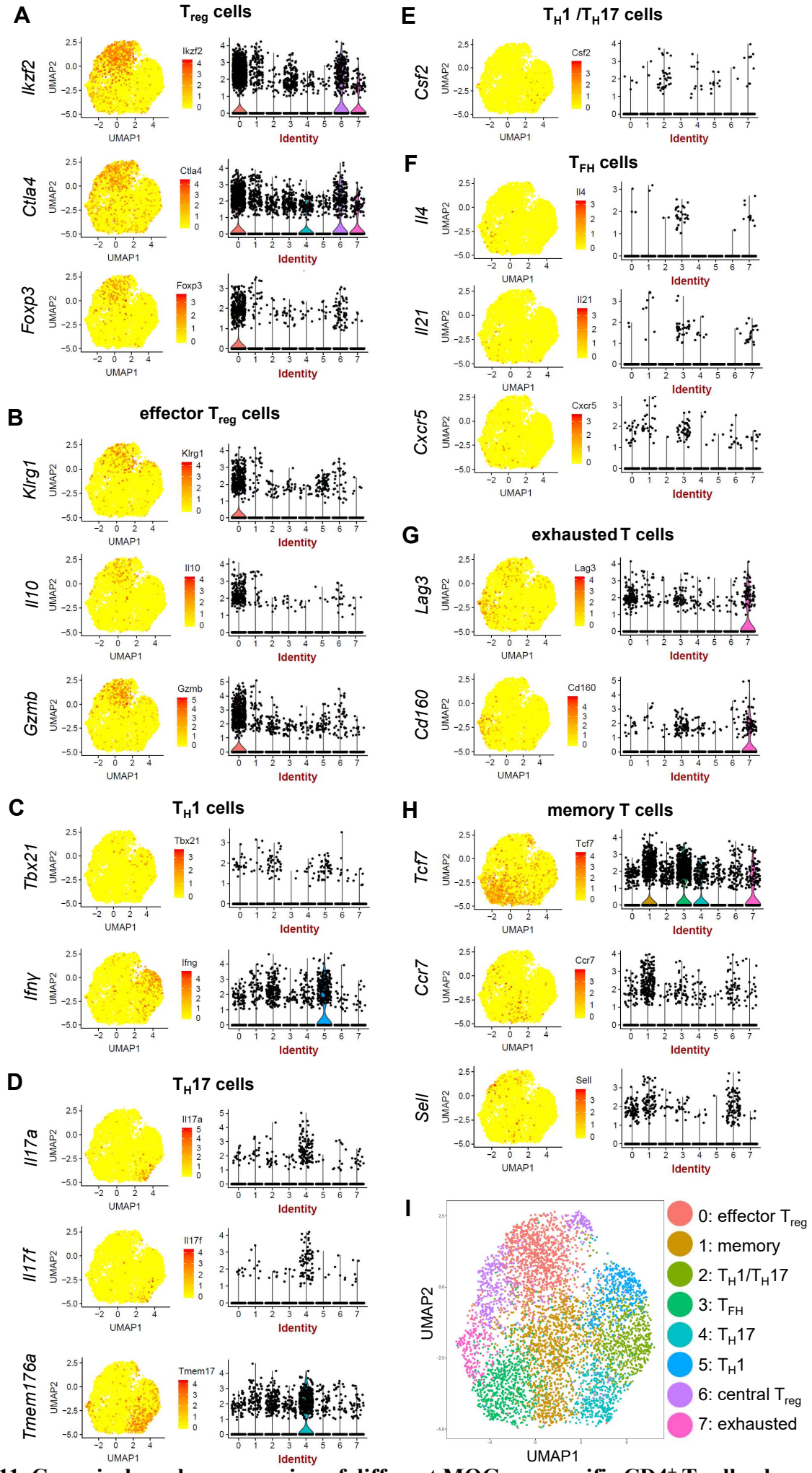

Fig. S11. Canonical marker expression of different MOG_{35-55}-specific $CD4^+$ T cell subpopulations.

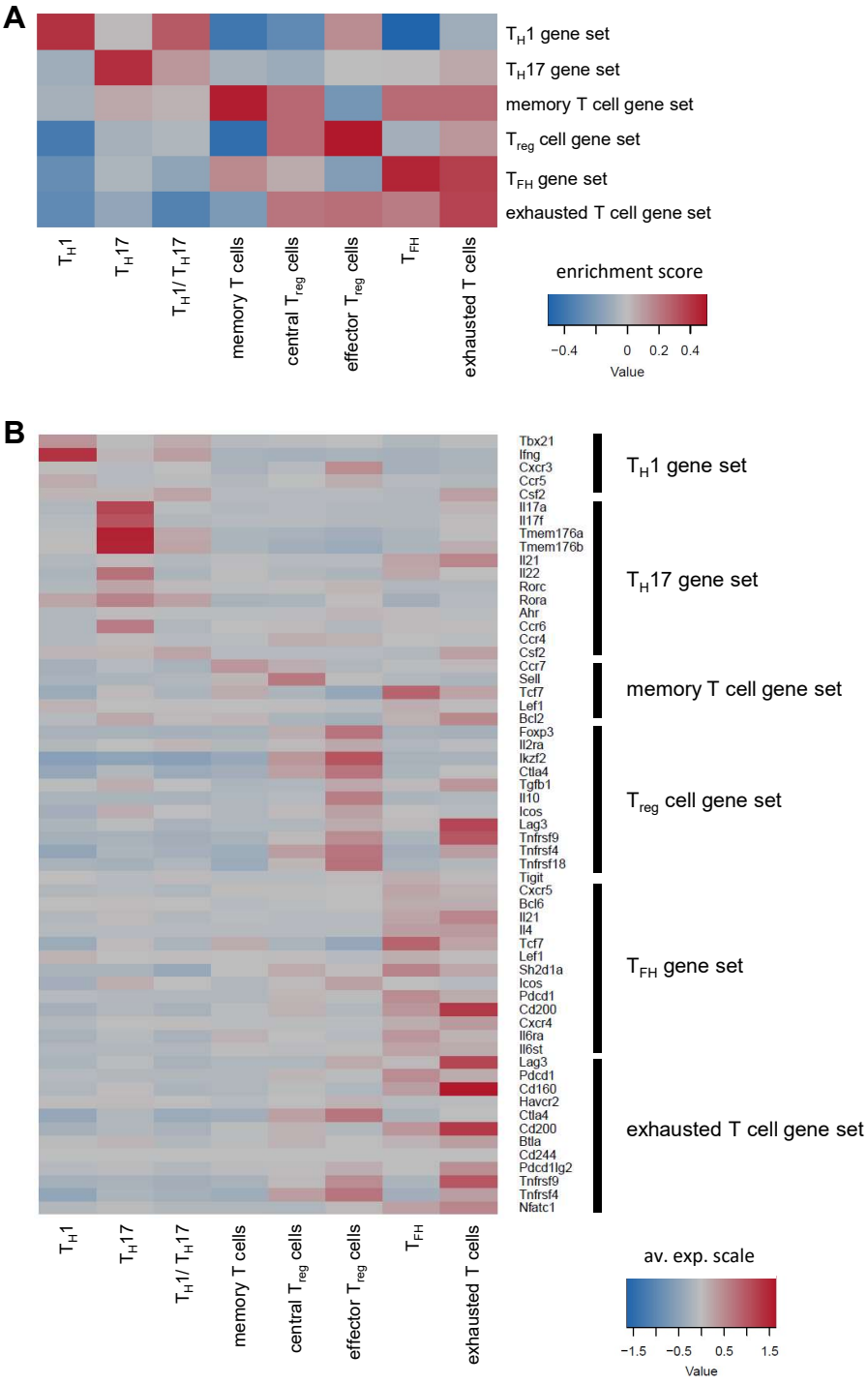

Fig. S12. Heatmap

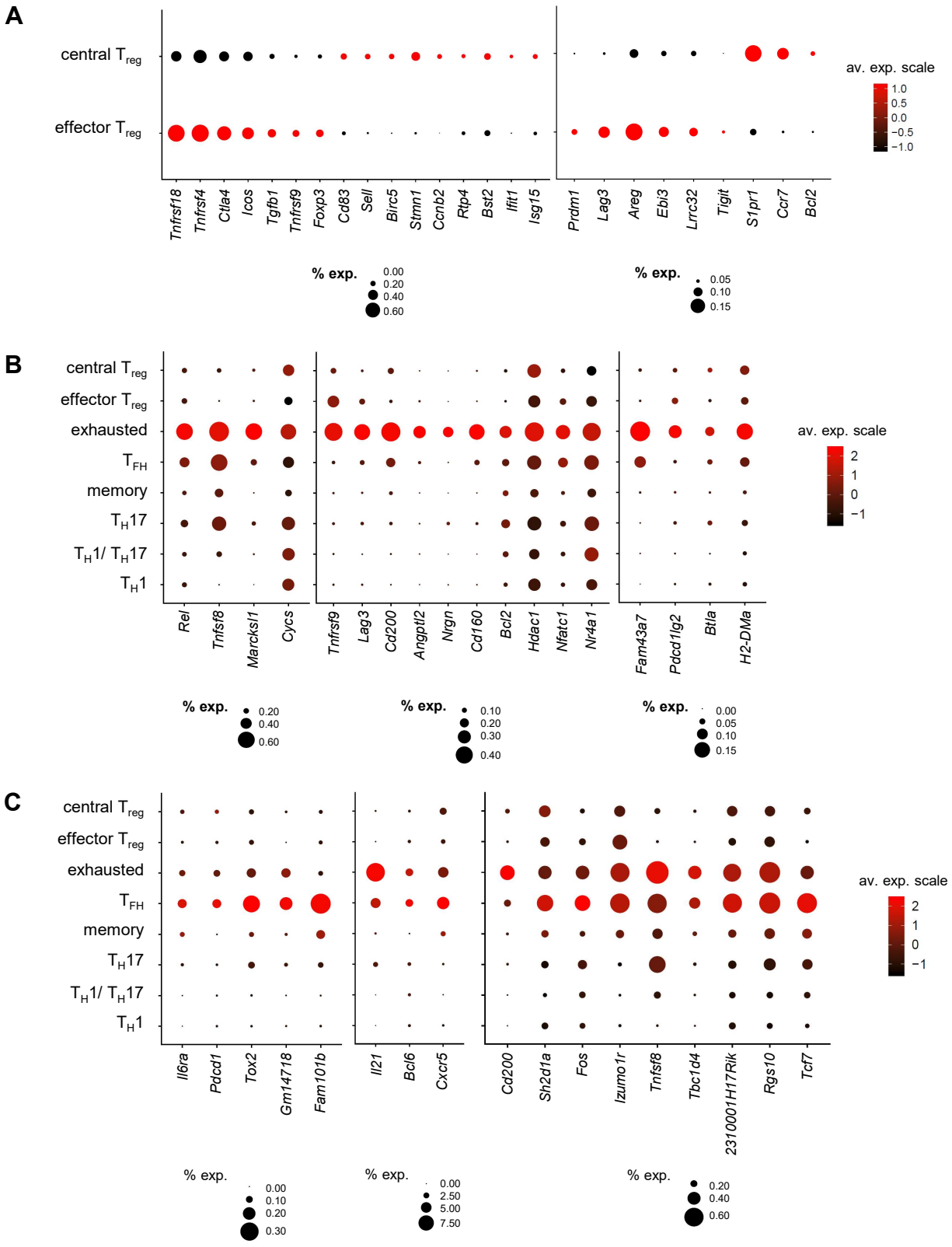

Fig. S13. Characterization of different MOG_{35-55}-specific $CD4^+$ T cell subpopulations revealed by single-cell RNA sequencing.

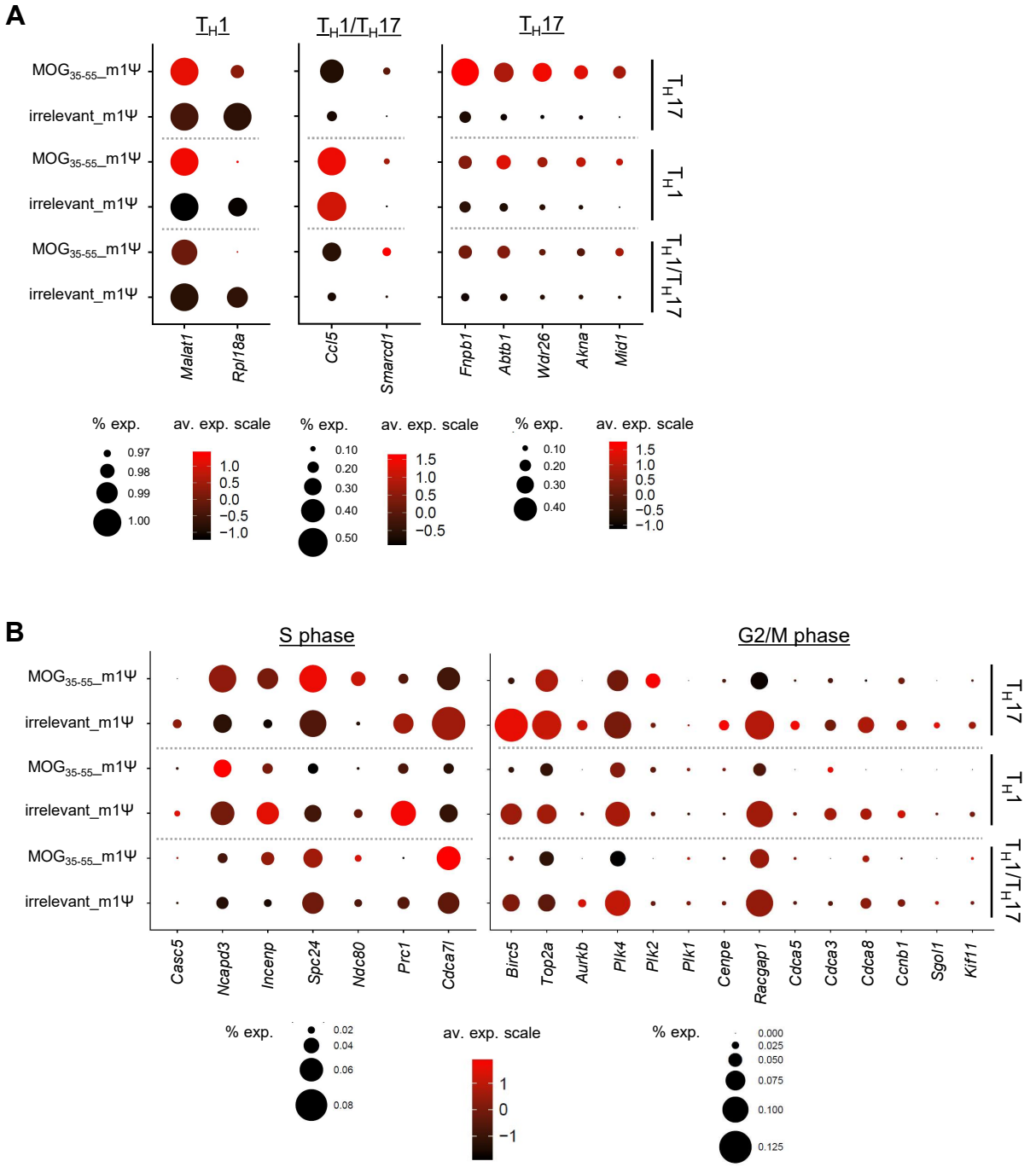

Fig. S14. Genes found to be differentially expressed in MOG_{35-55}-specific $CD4^+$ T cell subpopulations by single-cell RNA sequencing.

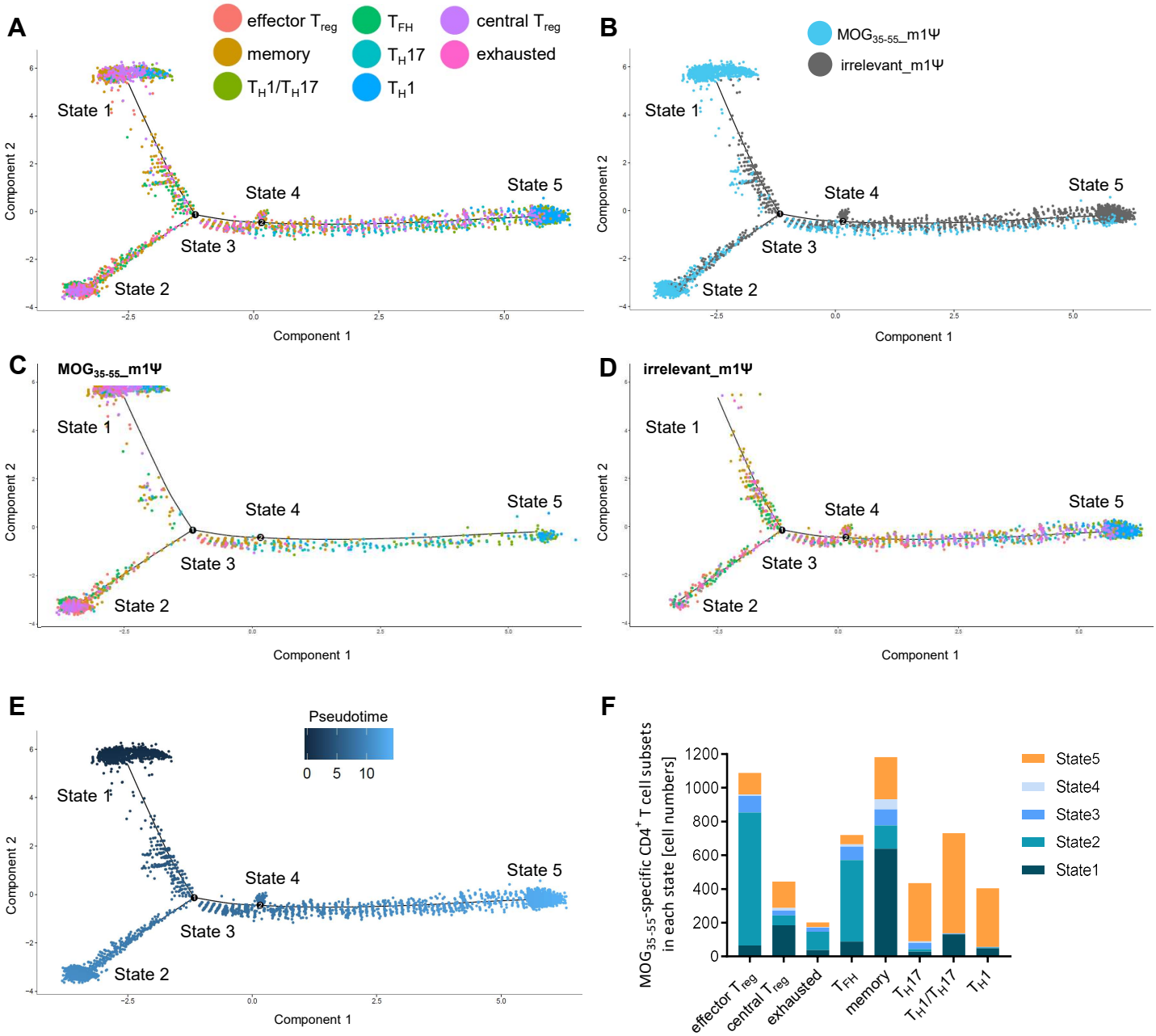

Fig. S15. Pseudotime ordering of MOG_{35-55}-specific $CD4^+$ T cells.

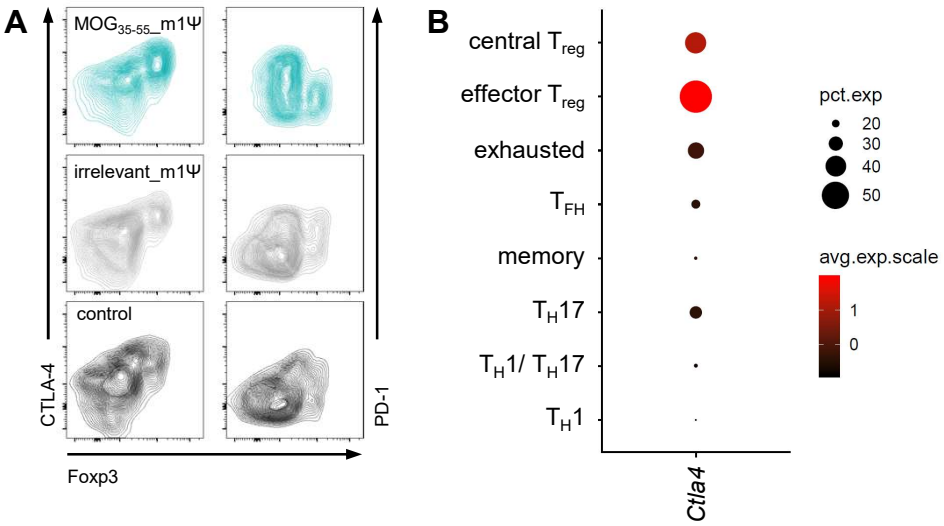

Fig. S16. Expression of Ctla4 and PD-1 on MOG_{35-55}-specific $CD4^+$ T_{reg} cells and T_{eff} cell subsets.

	MOG_{35-55}_m1Ψ	irrelevant_m1Ψ
Estimated number of cells	3,184	2,608
Mean reads per cell	252,137	139,257
Median gene per cell	817	1,021
Fraction reads in cells [%]	80.3	85.6
Median UMI counts per cell	1,387	1,915
Number of reads	802,806,269	363,184,718
Sequencing saturation [%]	98,5	96,5
Confidently mapped barcoded reads per cell [total]	303,844	166,040
Total cDNA amplification cycles	12	12

Table S1. Sequencing statistics.

Gene sets	Individual genes
T_H1 cells	Tbx21, Ifng, Cxcr3, Ccr5, Csf2
T_H17 cells	Il17a, Il17f, Tmem176a, Tmem176b, Il21, Il22, Rorc, Rora, Ahr, Ccr6, Ccr4, Csf2
memory T cells	Ccr7, Sell, Tcf7, Lef1, Bcl2
T_{reg} cells	Foxp3,Il2ra, Ikzf2, Ctla4, Tgfb1, Il10, Icos, Lag3, Tnfrsf9, Tnfrsf4, Tnfrsf18, Tigit
T_{FH} cells	Cxcr5, Bcl6, Il21, Il4, Tcf7, Lef1, Sh2d1a, Icos, Pdcd1, Cd200, Cxcr4, Il6ra , Il6st
exhausted T cells	Lag3, Pdcd1, Cd160, Havcr2, Ctla4, Cd200, Btla, Cd244, Pdcd1lg2, Tnfrsf9, Tnfrsf4, Nfatc1

Table S2. List of individual genes generating the subset-specific gene sets.

References and Notes

1. P. Serra, P. Santamaria, Antigen-specific therapeutic approaches for autoimmunity. *Nat. Biotechnol.* **37**, 238–251 (2019). doi:10.1038/s41587-019-0015-4 Medline

2. A. Miller, O. Lider, H. L. Weiner, Antigen-driven bystander suppression after oral administration of antigens. *J. Exp. Med.* **174**, 791–798 (1991). doi:10.1084/jem.174.4.791 Medline

3. L. M. Kranz, M. Diken, H. Haas, S. Kreiter, C. Loquai, K. C. Reuter, M. Meng, D. Fritz, F. Vascotto, H. Hefesha, C. Grunwitz, M. Vormehr, Y. Hüsemann, A. Selmi, A. N. Kuhn, J. Buck, E. Derhovanessian, R. Rae, S. Attig, J. Diekmann, R. A. Jabulowsky, S. Heesch, J. Hassel, P. Langguth, S. Grabbe, C. Huber, Ö. Türeci, U. Sahin, Systemic RNA delivery to dendritic cells exploits antiviral defence for cancer immunotherapy. *Nature* **534**, 396–401 (2016). doi:10.1038/nature18300 Medline

4. K. Karikó, M. Buckstein, H. Ni, D. Weissman, Suppression of RNA recognition by Toll-like receptors: The impact of nucleoside modification and the evolutionary origin of RNA. *Immunity* **23**, 165–175 (2005). doi:10.1016/j.immuni.2005.06.008 Medline

5. K. Karikó, H. Muramatsu, F. A. Welsh, J. Ludwig, H. Kato, S. Akira, D. Weissman, Incorporation of pseudouridine into mRNA yields superior nonimmunogenic vector with increased translational capacity and biological stability. *Mol. Ther.* **16**, 1833–1840 (2008). doi:10.1038/mt.2008.200 Medline

6. K. Karikó, H. Muramatsu, J. Ludwig, D. Weissman, Generating the optimal mRNA for therapy: HPLC purification eliminates immune activation and improves translation of nucleoside-modified, protein-encoding mRNA. *Nucleic Acids Res.* **39**, e142 (2011). doi:10.1093/nar/gkr695 Medline

7. N. Yogev, F. Frommer, D. Lukas, K. Kautz-Neu, K. Karram, D. Ielo, E. von Stebut, H.-C. Probst, M. van den Broek, D. Riethmacher, T. Birnberg, T. Blank, B. Reizis, T. Korn, H. Wiendl, S. Jung, M. Prinz, F. C. Kurschus, A. Waisman, Dendritic cells ameliorate autoimmunity in the CNS by controlling the homeostasis of PD-1 receptor(+) regulatory T cells. *Immunity* **37**, 264–275 (2012). doi:10.1016/j.immuni.2012.05.025 Medline

8. E. Bettelli, M. Pagany, H. L. Weiner, C. Linington, R. A. Sobel, V. K. Kuchroo, Myelin oligodendrocyte glycoprotein-specific T cell receptor transgenic mice develop spontaneous autoimmune optic neuritis. *J. Exp. Med.* **197**, 1073–1081 (2003). doi:10.1084/jem.20021603 Medline

9. I. S. Grewal, H. G. Foellmer, K. D. Grewal, H. Wang, W. P. Lee, D. Tumas, C. A. Janeway Jr., R. A. Flavell, CD62L is required on effector cells for local interactions in the CNS to cause myelin damage in experimental allergic encephalomyelitis. *Immunity* **14**, 291–302 (2001). doi:10.1016/S1074-7613(01)00110-8 Medline

10. Y. Arima, M. Harada, D. Kamimura, J. H. Park, F. Kawano, F. E. Yull, T. Kawamoto, Y. Iwakura, U. A. K. Betz, G. Márquez, T. S. Blackwell, Y. Ohira, T. Hirano, M. Murakami, Regional neural activation defines a gateway for autoreactive T cells to cross the blood-brain barrier. *Cell* **148**, 447–457 (2012). doi:10.1016/j.cell.2012.01.022 Medline

11. A. Reboldi, C. Coisne, D. Baumjohann, F. Benvenuto, D. Bottinelli, S. Lira, A. Uccelli, A. Lanzavecchia, B. Engelhardt, F. Sallusto, C-C chemokine receptor 6-regulated entry of TH-17 cells into the CNS through the choroid plexus is required for the initiation of EAE. *Nat. Immunol.* **10**, 514–523 (2009). doi:10.1038/ni.1716 Medline

12. S. Noor, E. H. Wilson, Role of C-C chemokine receptor type 7 and its ligands during neuroinflammation. *J. Neuroinflammation* **9**, 77 (2012). doi:10.1186/1742-2094-9-77 Medline

13. L. R. Shiow, D. B. Rosen, N. Brdicková, Y. Xu, J. An, L. L. Lanier, J. G. Cyster, M. Matloubian, CD69 acts downstream of interferon-α/β to inhibit S1P1 and lymphocyte egress from lymphoid organs. *Nature* **440**, 540–544 (2006). doi:10.1038/nature04606 Medline

14. R. Gold, C. Linington, H. Lassmann, Understanding pathogenesis and therapy of multiple sclerosis via animal models: 70 years of merits and culprits in experimental autoimmune encephalomyelitis research. *Brain* **129**, 1953–1971 (2006). doi:10.1093/brain/awl075 Medline

15. C. P. Genain, K. Abel, N. Belmar, F. Villinger, D. P. Rosenberg, C. Linington, C. S. Raine, S. L. Hauser, Late complications of immune deviation therapy in a nonhuman primate. *Science* **274**, 2054–2057 (1996). doi:10.1126/science.274.5295.2054 Medline

16. N. Pardi, K. Parkhouse, E. Kirkpatrick, M. McMahon, S. J. Zost, B. L. Mui, Y. K. Tam, K. Karikó, C. J. Barbosa, T. D. Madden, M. J. Hope, F. Krammer, S. E. Hensley, D. Weissman, Nucleoside-modified mRNA immunization elicits influenza virus hemagglutinin stalk-specific antibodies. *Nat. Commun.* **9**, 3361 (2018). doi:10.1038/s41467-018-05482-0 Medline

17. E. Cretney, A. Kallies, S. L. Nutt, Differentiation and function of Foxp3(+) effector regulatory T cells. *Trends Immunol.* **34**, 74–80 (2013). doi:10.1016/j.it.2012.11.002 Medline

18. R. J. Miragaia, T. Gomes, A. Chomka, L. Jardine, A. Riedel, A. N. Hegazy, N. Whibley, A. Tucci, X. Chen, I. Lindeman, G. Emerton, T. Krausgruber, J. Shields, M. Haniffa, F. Powrie, S. A. Teichmann, Single-Cell Transcriptomics of Regulatory T Cells Reveals Trajectories of Tissue Adaptation. *Immunity* **50**, 493–504.e7 (2019). doi:10.1016/j.immuni.2019.01.001 Medline

19. N. Paschalidis, A. J. Iqbal, F. Maione, E. G. Wood, M. Perretti, R. J. Flower, F. D'Acquisto, Modulation of experimental autoimmune encephalomyelitis by endogenous annexin A1. *J. Neuroinflammation* **6**, 33 (2009). doi:10.1186/1742-2094-6-33 Medline

20. S. A. Apostolidis, T. Rauen, C. M. Hedrich, G. C. Tsokos, J. C. Crispín, Protein phosphatase 2A enables expression of interleukin 17 (IL-17) through chromatin remodeling. *J. Biol. Chem.* **288**, 26775–26784 (2013). doi:10.1074/jbc.M113.483743 Medline

21. A. Collison, L. Hatchwell, N. Verrills, P. A. B. Wark, A. P. de Siqueira, M. Tooze, H. Carpenter, A. S. Don, J. C. Morris, N. Zimmermann, N. W. Bartlett, M. E. Rothenberg, S. L. Johnston, P. S. Foster, J. Mattes, The E3 ubiquitin ligase midline 1 promotes allergen and rhinovirus-induced asthma by inhibiting protein phosphatase 2A activity. *Nat. Med.* **19**, 232–237 (2013). doi:10.1038/nm.3049 Medline

22. E. E. Kara, D. R. McKenzie, C. R. Bastow, C. E. Gregor, K. A. Fenix, A. D. Ogunniyi, J. C. Paton, M. Mack, D. R. Pombal, C. Seillet, B. Dubois, A. Liston, K. P. A. MacDonald, G. T. Belz, M. J. Smyth, G. R. Hill, I. Comerford, S. R. McColl, CCR2 defines in vivo development and homing of IL-23-driven GM-CSF-producing Th17 cells. *Nat. Commun.* **6**, 8644 (2015). doi:10.1038/ncomms9644 Medline

23. B. T. Fife, G. B. Huffnagle, W. A. Kuziel, W. J. Karpus, CC chemokine receptor 2 is critical for induction of experimental autoimmune encephalomyelitis. *J. Exp. Med.* **192**, 899–906 (2000). doi:10.1084/jem.192.6.899 Medline

24. S. Glatigny, R. Duhen, M. Oukka, E. Bettelli, Cutting edge: Loss of α4 integrin expression differentially affects the homing of Th1 and Th17 cells. *J. Immunol.* **187**, 6176–6179 (2011). doi:10.4049/jimmunol.1102515 Medline

25. C. Runne, S. Chen, WD40-repeat proteins control the flow of Gβγ signaling for directional cell migration. *Cell Adh. Migr.* **7**, 214–218 (2013). doi:10.4161/cam.22940 Medline

26. T. Kinashi, K. Katagiri, Regulation of lymphocyte adhesion and migration by the small GTPase Rap1 and its effector molecule, RAPL. *Immunol. Lett.* **93**, 1–5 (2004). doi:10.1016/j.imlet.2004.02.008 Medline

27. C. C. Lin, T. R. Bradstreet, E. A. Schwarzkopf, J. Sim, J. A. Carrero, C. Chou, L. E. Cook, T. Egawa, R. Taneja, T. L. Murphy, J. H. Russell, B. T. Edelson, Bhlhe40 controls cytokine production by T cells and is essential for pathogenicity in autoimmune neuroinflammation. *Nat. Commun.* **5**, 3551 (2014). doi:10.1038/ncomms4551 Medline

28. B. R. Burton, G. J. Britton, H. Fang, J. Verhagen, B. Smithers, C. A. Sabatos-Peyton, L. J. Carney, J. Gough, S. Strobel, D. C. Wraith, Sequential transcriptional changes dictate safe and effective antigen-specific immunotherapy. *Nat. Commun.* **5**, 4741 (2014). doi:10.1038/ncomms5741 Medline

29. L. M. Yshii, R. Hohlfeld, R. S. Liblau, Inflammatory CNS disease caused by immune checkpoint inhibitors: Status and perspectives. *Nat. Rev. Neurol.* **13**, 755–763 (2017). doi:10.1038/nrneurol.2017.144 Medline

30. L. Wang, K. Pino-Lagos, V. C. de Vries, I. Guleria, M. H. Sayegh, R. J. Noelle, Programmed death 1 ligand signaling regulates the generation of adaptive Foxp3+CD4+ regulatory T cells. *Proc. Natl. Acad. Sci. U.S.A.* **105**, 9331–9336 (2008). doi:10.1073/pnas.0710441105 Medline

31. N. Ohkura, S. Sakaguchi, Maturation of effector regulatory T cells. *Nat. Immunol.* **12**, 283–284 (2011). doi:10.1038/ni0411-283 Medline

32. A. M. Thornton, E. M. Shevach, Suppressor effector function of CD4+CD25+ immunoregulatory T cells is antigen nonspecific. *J. Immunol.* **164**, 183–190 (2000). doi:10.4049/jimmunol.164.1.183 Medline

33. X. Clemente-Casares, J. Blanco, P. Ambalavanan, J. Yamanouchi, S. Singha, C. Fandos, S. Tsai, J. Wang, N. Garabatos, C. Izquierdo, S. Agrawal, M. B. Keough, V. W. Yong, E. James, A. Moore, Y. Yang, T. Stratmann, P. Serra, P. Santamaria, Expanding antigen-specific regulatory networks to treat autoimmunity. *Nature* **530**, 434–440 (2016). doi:10.1038/nature16962 Medline

34. F. P. Legoux, J.-B. Lim, A. W. Cauley, S. Dikiy, J. Ertelt, T. J. Mariani, T. Sparwasser, S. S. Way, J. J. Moon, CD4+ T Cell Tolerance to Tissue-Restricted Self Antigens Is Mediated by Antigen-Specific Regulatory T Cells Rather Than Deletion. *Immunity* **43**, 896–908 (2015). doi:10.1016/j.immuni.2015.10.011 Medline

35. N. Dammes, D. Peer, Paving the Road for RNA Therapeutics. *Trends Pharmacol. Sci.* **41**, 755–775 (2020). doi:10.1016/j.tips.2020.08.004 Medline

36. U. Sahin, Ö. Türeci, Personalized vaccines for cancer immunotherapy. *Science* **359**, 1355–1360 (2018). doi:10.1126/science.aar7112 Medline

37. U. Sahin, E. Derhovanessian, M. Miller, B. P. Kloke, P. Simon, M. Löwer, V. Bukur, A. D. Tadmor, U. Luxemburger, B. Schrörs, T. Omokoko, M. Vormehr, C. Albrecht, A. Paruzynski, A. N. Kuhn, J. Buck, S. Heesch, K. H. Schreeb, F. Müller, I. Ortseifer, I. Vogler, E. Godehardt, S. Attig, R. Rae, A. Breitkreuz, C. Tolliver, M. Suchan, G. Martic, A. Hohberger, P. Sorn, J. Diekmann, J. Ciesla, O. Waksmann, A. K. Brück, M. Witt, M. Zillgen, A. Rothermel, B. Kasemann, D. Langer, S. Bolte, M. Diken, S. Kreiter, R. Nemecek, C. Gebhardt, S. Grabbe, C. Höller, J. Utikal, C. Huber, C. Loquai, Ö. Türeci, Personalized RNA mutanome vaccines mobilize poly-specific therapeutic immunity against cancer. *Nature* **547**, 222–226 (2017). doi:10.1038/nature23003 Medline

38. S. Kreiter, A. Selmi, M. Diken, M. Sebastian, P. Osterloh, H. Schild, C. Huber, O. Türeci, U. Sahin, Increased antigen presentation efficiency by coupling antigens to MHC class I trafficking signals. *J. Immunol.* **180**, 309–318 (2008). doi:10.4049/jimmunol.180.1.309 Medline

39. T. Beissert, M. Perkovic, A. Vogel, S. Erbar, K. C. Walzer, T. Hempel, S. Brill, E. Haefner, R. Becker, Ö. Türeci, U. Sahin, A Trans-amplifying RNA Vaccine Strategy for Induction of Potent Protective Immunity. *Mol. Ther.* **28**, 119–128 (2020). doi:10.1016/j.ymthe.2019.09.009 Medline

40. M. Baiersdörfer, G. Boros, H. Muramatsu, A. Mahiny, I. Vlatkovic, U. Sahin, K. Karikó, A facile method for removal of dsRNA contaminant from in vitro-transcribed mRNA. *Mol. Ther. Nucleic Acids* **15**, 26–35 (2019). doi:10.1016/j.omtn.2019.02.018 Medline

41. D. Weissman, N. Pardi, H. Muramatsu, K. Karikó, HPLC purification of in vitro transcribed long RNA. *Methods Mol. Biol.* **969**, 43–54 (2013). doi:10.1007/978-1-62703-260-5_3 Medline

42. S. Holtkamp, S. Kreiter, A. Selmi, P. Simon, M. Koslowski, C. Huber, O. Türeci, U. Sahin, Modification of antigen-encoding RNA increases stability, translational efficacy, and T-cell stimulatory capacity of dendritic cells. *Blood* **108**, 4009–4017 (2006). doi:10.1182/blood-2006-04-015024 Medline

43. A. B. Vogel, L. Lambert, E. Kinnear, D. Busse, S. Erbar, K. C. Reuter, L. Wicke, M. Perkovic, T. Beissert, H. Haas, S. T. Reece, U. Sahin, J. S. Tregoning, Self-Amplifying RNA Vaccines Give Equivalent Protection against Influenza to mRNA Vaccines but at Much Lower Doses. *Mol. Ther.* **26**, 446–455 (2018). doi:10.1016/j.ymthe.2017.11.017 Medline

44. G. X. Y. Zheng, J. M. Terry, P. Belgrader, P. Ryvkin, Z. W. Bent, R. Wilson, S. B. Ziraldo, T. D. Wheeler, G. P. McDermott, J. Zhu, M. T. Gregory, J. Shuga, L. Montesclaros, J. G.

Underwood, D. A. Masquelier, S. Y. Nishimura, M. Schnall-Levin, P. W. Wyatt, C. M. Hindson, R. Bharadwaj, A. Wong, K. D. Ness, L. W. Beppu, H. J. Deeg, C. McFarland, K. R. Loeb, W. J. Valente, N. G. Ericson, E. A. Stevens, J. P. Radich, T. S. Mikkelsen, B. J. Hindson, J. H. Bielas, Massively parallel digital transcriptional profiling of single cells. *Nat. Commun.* **8**, 14049 (2017). doi:10.1038/ncomms14049 Medline

45. A. Butler, P. Hoffman, P. Smibert, E. Papalexi, R. Satija, Integrating single-cell transcriptomic data across different conditions, technologies, and species. *Nat. Biotechnol.* **36**, 411–420 (2018). doi:10.1038/nbt.4096 Medline

46. I. Tirosh, B. Izar, S. M. Prakadan, M. H. Wadsworth 2nd, D. Treacy, J. J. Trombetta, A. Rotem, C. Rodman, C. Lian, G. Murphy, M. Fallahi-Sichani, K. Dutton-Regester, J. R. Lin, O. Cohen, P. Shah, D. Lu, A. S. Genshaft, T. K. Hughes, C. G. Ziegler, S. W. Kazer, A. Gaillard, K. E. Kolb, A. C. Villani, C. M. Johannessen, A. Y. Andreev, E. M. Van Allen, M. Bertagnolli, P. K. Sorger, R. J. Sullivan, K. T. Flaherty, D. T. Frederick, J. Jané-Valbuena, C. H. Yoon, O. Rozenblatt-Rosen, A. K. Shalek, A. Regev, L. A. Garraway, Dissecting the multicellular ecosystem of metastatic melanoma by single-cell RNA-seq. *Science* **352**, 189–196 (2016). doi:10.1126/science.aad0501 Medline

47. L. Waltman, N. J. Van Eck, A smart local moving algorithm for large-scale modularity-based community detection. *Eur. Phys. J. B* **86**, 471 (2013). doi:10.1140/epjb/e2013-40829-0

48. L. McInnes, J. Healy, J. Melville, UMAP: Uniform Manifold Approximation and Projection for Dimension Reduction. arXiv:1802.03426 [stat.ML] (9 February 2018).

49. E. Becht, L. McInnes, J. Healy, C. A. Dutertre, I. W. H. Kwok, L. G. Ng, F. Ginhoux, E. W. Newell, Dimensionality reduction for visualizing single-cell data using UMAP. *Nat. Biotechnol.* **37**, 38–44 (2019). doi:10.1038/nbt.4314 Medline

50. S. Hänzelmann, R. Castelo, J. Guinney, GSVA: Gene set variation analysis for microarray and RNA-seq data. *BMC Bioinformatics* **14**, 7 (2013). doi:10.1186/1471-2105-14-7 Medline

51. C. Trapnell, D. Cacchiarelli, J. Grimsby, P. Pokharel, S. Li, M. Morse, N. J. Lennon, K. J. Livak, T. S. Mikkelsen, J. L. Rinn, The dynamics and regulators of cell fate decisions are revealed by pseudotemporal ordering of single cells. *Nat. Biotechnol.* **32**, 381–386 (2014). doi:10.1038/nbt.2859 Medline

52. X. Qiu, Q. Mao, Y. Tang, L. Wang, R. Chawla, H. A. Pliner, C. Trapnell, Reversed graph embedding resolves complex single-cell trajectories. *Nat. Methods* **14**, 979–982 (2017). doi:10.1038/nmeth.4402 Medline